Conductor to insulator transition and insulator to conductor transition, studied by gas discharges and breakjunctions

Conductor to insulator transition and insulator to conductor transition, studied by gas discharges and breakjunctions

een wetenschappelijke proeve op het gebied van de
Natuurwetenschappen, Wiskunde en Informatica

Proefschrift

ter verkrijging van de graad van doctor
aan de Katholieke Universiteit Nijmegen,
op gezag van de Rector Magnificus Prof.dr. C.W.P.M. Blom,
volgens besluit van het College van Decanen
in het openbaar te verdedigen op
vrijdag 26 maart 2004
des namiddags om 1.30 uur precies

door

Godfried Cornelius Gerardus Maria Manders

geboren op 19 juli 1974
te Sittard

Promotor:	Prof. Dr. Ir. J. C. Maan
Co-Promotor:	Dr. P. C. M. Christianen
Manuscriptcommissie:	Prof. Dr. U. Ebert (Technische Universiteit Eindhoven)
	Dr. N. Dam
	Dr. U. Zeitler

ISBN 90-9017787-6

Voorwoord

Het is een regenachtige dag in december en eindelijk kan ik beginnen met het schrijven van het voorwoord. Toen ik bijna 7 jaar geleden aan dit promotieonderzoek begon had ik niet gedacht dat het zo'n lange strijd zou worden. Maar zoals Fredrick Douglas al voor mij zei: "zonder strijd is er geen vooruitgang". En dus heb ik altijd voor ogen gehouden dat eens dit boekje klaar zou zijn en dat het hopelijk een aantal leuke, nieuwe wetenschappelijke dingen zou laten zien. Terugdenkend aan hoe ik 7 jaar geleden begon, besef ik hoeveel er in de afgelopen periode is gebeurd, zowel positief als negatief. Maar gelukkig waren er een hoop goede vrienden waarop ik steeds kon terugvallen en die ervoor gezorgd hebben dat uiteindelijk toch nog een boekje gepubliceerd kon worden. Het minste wat ik voor jullie terug kan doen is jullie bedanken.

Het begon dus ongeveer 7 jaar geleden, toen ik met Jan Kees een gesprek had over een mogelijke promotieplaats binnen het magnetenlab. Hij liet me toen spectaculaire plaatjes zien van vonken in een magneetveld. Vanaf dat moment wist ik dat ik dit wilde gaan doen: lekker spelen met hoogspanning.

De dagelijks begeleiding heeft Peter Cristianen op zich genomen. Peter bedankt dat jouw deur altijd open stond en dat je altijd probeerde mee te denken en mij in de goede richting probeerde te duwen.

Op het moment dat ik het niet meer zag zitten met vonkjes in een magneetveld heeft Andrey Geim me gelukkig uit het diepe dal gered. Andrey thank you for bringing up the idea for measuring quantized conduction in magnetic field and all the support. Nadat dit experiment wel lukte en er leuke resultaten waren, was ik vast besloten om de vonkjes in een magneetveld ook tot een succes te maken.

De vorige drie mensen waren vooral verantwoordelijk voor de fysische ideeën. Zonder de drie mensen die ik nu ga noemen waren deze ideeën

nooit uitgevoerd en was dit boekje nooit geschreven. Om te beginnen, Lijnis bedankt dat je altijd bereid was om mijn kladtekeningen van de vonkenkamer en triggerkamer uit te werken tot de mooie tekening (zoals te zien is dit boekje). Tevens ook bedankt voor het maken en verbeteren van deze instrumenten, ondanks dat ik ze elke keer weer vol met silicone, lijm en tape smeerde. Hung zonder jouw data acquisition programma's was ik volgens mij nu nog steeds goud stapjes in een magneetveld aan het meten. Laatste in dit rijtje is Henk. Henk bedankt voor de goede zorgen, zonder jou was ik zeker een keer aan de hoogspanning blijven hangen. Tevens ook bedankt voor het luisterend oor over looptijden over kabels en pulse lengtes enz.
Harry bedankt dat de magneten het altijd deden, ondanks mijn vonken en dat er altijd genoeg ijs was.
Zonder de administratieve hulp van Ine en Martha zou het regelmatig een organisatorische puinhoop zijn geworden binnen het lab. Martha tevens bedankt voor de steun en de schouder op de zware momenten.
Dan zijn er natuurlijk de mede AIO's/OIO's die allemaal in hetzelfde schuitje zitten en elkaar steunen. Cecile, Maaike en Eric bedankt voor alle steun en alle babysit uren. Ik denk dat we gelukkig ook een hoop leuke moment gedeeld hebben, aan de waalkade en tijdens de lunches. Maaike ook nog bedankt voor het twee keer laten quenchen van de magneet; dit was behoorlijk spectaculair. I was lucky to be in a lab. with lots of foreigners with there own habits and culture. Cecilia, Fabio, Igor, Kostya and Marius thank you for all the nice conversations we had and for the help.
Jos R, Stef W, Jos P, Stef O, Jan, Adri, Alex, Sjoerd, Andrea, bedankt voor de gezellige koffiepauzes en de gezellige sfeer op het lab.

Mijn collega's bij Philips wil ik bedanken voor het steeds maar weer blijven vragen naar de stand van zaken van het boekje, waardoor ik steeds weer gepushed werd om door te werken, in het bijzonder Ruud, John, Yvonne, Bram, Huub en Sjef.
Op de momenten dat ik niet aan het meten was waren er gelukkig een hoop mensen waarmee ik een heleboel gezellige dingen gedaan heb.
Jan Willem vanaf het moment dat we samen in het mentorgroepje bij natuurkunde zaten hebben we een hoop lol en ook de nodige steun aan elkaar gehad, bedankt hiervoor.

Cristel, je hebt 3 jaar lang altijd verhalen moeten aanhoren over experimenten die maar niet wilde lukken maar jij wist me toch steeds weer op te monteren, bedankt.
Arthur en Patrick, ik ben altijd weer blij dat ik op onze vriendschap kan terugvallen op de momenten dat het nodig is.
Marjo, jij was de afgelopen 2 jaar de motor achter dit boekje. Jij wist me steeds weer te motiveren om in de avonduren toch maar weer achter de computer te kruipen, dankzij jouw liefde en steun is het boekje toch afgekomen.

Zonder de steun van mijn ouders, zus en Ingo weet ik zeker dat ik het nooit zover geschopt zou hebben. Zij hebben altijd vertrouwen in me gehad en zijn er altijd voor me geweest, bedankt hiervoor.

Contents

Chapter 1

General introduction to conduction

Introduction

Already in prehistoric times people were familiar with electrical phenomena, in particular through thunder and lightning which have played an enormous role in many cultures and have lead to fear and respect for the thunder god. On a smaller scale, four thousand years ago, the Egyptians already drew pictures of how an electric eel killed other animals using an electric shock, even though they were of course not familiar with the phenomenon electricity. The Greek philosopher Thales of Milete described around 600 before Christ how yellow amber after polishing could attract small objects like wool and chicken feathers, an effect which we now know may be attributed to static electricity. In Roman times, doctors tried to heal people with electrical fish. Till about 300 years ago these phenomena stood mostly on their own and no systematic experimental studies were done.
With the advent of experimental physics at the time of Galileo a more scientific approach to study these phenomena was developed. In 1663 Otto von Guericke discovered that a strange glow appeared when he held his hand against a turning ball of sulfur. The sulfurball could attract small objects and sometimes small sparks appeared. This discovery led to the

invention of the electrical machine, with which it was possible to create electrical effects inside a laboratory in a more controlled fashion. From this moment on many physicists contributed to unriddle the electrical phenomena [1].
In 1729, Stephen Gray discovered the existence of conductors and insulators, shortly followed by Charles François de Cisternay who demonstrated in 1733 that there were two kind of electrical charges: positive and negative. In 1746, Pieter van Musschenbroek discovered the "Leidse fles"in which it was possible to store a great amount of charge. In 1752, Benjamin Franklin let a kite up in a thunderstorm and showed that lighting is an electrical spark and that therefore this natural effect could be linked to the electrical phenomena now being studied in the laboratory.
All of these discoveries did not have any practical use and were all done in gases. However, when Luigi Galvani showed that there is a voltage between two metallic plates when they are placed in a salt solution, this situation changed. Galvani's discovery lead to the first battery by Volta, which made it possible to study electrical current, which eventually has lead to the famous laws of Ohm, Ampère, Faraday, Joule and Maxwell, all in the 19^{th} century.
Although the phenomena were by now reasonably well understood, real insight in their microscopic origin became only possible around 1897 when Joseph John Thomson discovered the electron as a particle with a fixed charge. A proper theory of electronic conduction became possible with the foundation of quantum mechanics after Bohr made his atom theory in 1913. With this theory conduction through metals was described by P. Drude. He first suggested a model that assumed that an electron behaves like a classical gas. In 1928 Sommerfeld modified the Drude theory to take degeneracy into account allowing to describe conduction through metals in an approximate but fundamentally correct fashion.
Throughout history two kinds of materials appear: Insulators, which are materials in which charges are mostly bound and immobile (gases and also semiconductors which may be considered as poor insulators), and conductors, which are materials in which charges may move freely (metals).
Conduction occurs when many charge carriers move freely and in a metal there are about 10^{23} cm^{-3} [2] free charge carriers, which makes it a good conductor. On the other hand in a gas there are only around 100 cm^{-3} [3] free charge carriers and a gas conducts very poorly. However, when a high

electric field is applied to a gas, the electrons which are normally bound to their atoms may be liberated through collisions and the insulator becomes a conductor. On the other hand when a metal wire is thinned to the point that it is reduced to a single chain of metallic atoms, there will be a point when the conduction disappears and the contact becomes insulating. In this thesis we study these two distinct phenomena, which one might call the onset and the disappearance of conduction.
This thesis is divided into two parts. In the first part, we will show how an insulator (gas) is transformed into a very good conductor by applying a very high electric field. In chapter 2 we give an introduction to this so-called gas discharge physics. Chapter 3 shows the experimental setup which is used, with special emphasis on the techniques which require very fast data acquisition since this gas-breakdown is extremely fast (a few nsec.). In chapter 4 the propagation measurements for positive and negative discharges are described and chapter 5 shows the velocity of the discharge. Finally in chapter 6 the effect of a magnetic field applied on the discharge is discussed.
In the second part of the thesis we study how conductance disappears when a metal (gold) contact is interrupted (chapter 7). This disappearance of conductance is associated with the observation of quantized conductance steps and we study the effect of a magnetic field on these steps.

1.1 Bibliography

[1] J. Masschelein, P. Cox, J. Moors and W. van den Munckho, *Fysica deel 5*, (Malmberg, Den Bosch, 1990).

[2] Harald Ibach, Hans Lüth, *Solid state physics*, (Springer, New York, 1993).

[3] W.F.L.M. Houben *Pulsed corona-Induced degradation of organic materials in water* thesis University of Eindhoven, 2000.

Part I

Streamer formation and propagation in Gas Discharges

Chapter 2

Introduction to gas discharges

Introduction

Gases are generally considered to be insulators, but the appearance of lightning in the earths atmosphere shows that they may became good conductors under appropriate conditions. Already in the 18^{th}century Coulomb [1] came to the conclusion, performing experiments on the loss of electricity from a charged body suspended by insulating strings, that air was not such a perfect insulator, since he observed leakage of the charge. In the 19^{th} century powerful electric batteries were developed, which allowed the discovery of arc discharges, first observed by Petrov [2]. The arc was created by bringing two oppositely charged carbon electrodes into contact and then separating them. Around 1830 Faraday discovered and studied the glow discharge. He worked with tubes evacuated to a pressure p of about 1 Torr and applied voltages of up to 1000 V.
The development of the physics of gas discharges in the late 19^{th} and early 20^{th} centuries is inseparable from the increasing understanding of atomic physics. After Crooke's cathode ray experiments and Thomson's measurements of the e/m ratio (electron charge e over its mass m), it became clear that the current in gases is mostly carried by the few free electrons that are still present at room temperature. At the same time knowledge about elementary processes involving electrons, ions and atoms were in fact mainly obtained by studying physical phenomena of gas discharges.

In the beginning of 1900 Townsend discovered the laws governing the ionization of the gas and the subsequent discharge (known as the Townsend discharge, see next section) in an uniform electric field. Numerous experimental results were gradually accumulated, resulting in the determination of important parameters, such as the cross sections of various electron-atom collisions, the drift velocities of electrons and ions and their recombination coefficients [3]. This work has built the foundations of the current reference sources and constituted the first systematic investigations of the physics of gas discharges.
The theory of Townsend describing discharges works very well for uniform electric fields that are not too high, and at low pressures. In most practical cases however, non-uniform electrode configurations, high pressures and high electric fields are used. In this case a substantial amount of ionization takes place, which leads to an appreciable space charge (due to both free electrons and charged ions) and therefore to non-uniform fields, for which Townsend results are not applicable. The behavior of the discharge is then mainly governed by the electric field determined by the space charge itself, rather than by the original applied electric field. For this reason the theory of Townsend cannot explain some experimental observations, such as the fact that usually the formation time of the fully developed discharge (breakdown) is shorter than the transition time of ions and electrons between the electrodes.
To describe breakdown at higher pressures and voltages Meek [4] and Raether [5] proposed in 1940 the so-called streamer theory of breakdown. The main difference with the Townsend discharge is that the field distortion due to a concentrated large positive space charge in a certain volume cannot be neglected. An avalanche of typically more than 10^8 electrons is called a streamer and is more than sufficient to draw in new avalanches from more distant points in the gap between the electrodes. The merging of these induced avalanches creates a rapidly propagating filamentary ionized channel; the streamer. Clearly the streamer propagation is radically different from the Townsend model, since one may say that the streamer propagates to some extend in its own electric field,which has little relation to the original electric field that initiated the discharge. Lightning can propagate over such long distances, because the high voltage at its tip ionizes the air in front of it, which allows the tip to propagate and to create its own discharge channel.

Finally in the last phase of the discharge, the ionized channel becomes a neutral plasma consisting of equal amounts of positive and negative charges. This channel transfers the electrostatic potential from the origin towards the propagating tip. The typical lightning discharges seen during a thunderstorm are the current pulses along the formed channel. Experimental and theoretical work in the last years was largely devoted to understand the conditions for streamer formation, the characteristics of their propagation [6-14].

2.1 Theory

In theory there are a few explanation of how a gas discharge can start and can lead to a breakdown. In this section we describe two of them, one at low pressures and low voltage (Townsend breakdown) and one at high pressures and high voltage (streamer breakdown).

2.1.1 Townsend breakdown

Consider a volume filled with gas, between a flat cathode at potential zero, and a flat anode at a distance d at a high dc potential V_a. Under these conditions the electric field is constant and the potential drops linearly. When due to an external cause, a free electron is formed, for instance by ionization of an atom by cosmic radiation, or through emission of an electron from the cathode due to light, this free electron will be accelerated towards the anode. As soon as this electron has gained a sufficient amount of energy, it may ionize an atom, leaving one ion and two electrons. Both ions and electrons are in turn accelerated, after which this can lead to further ionization. Eventually this mechanism can create an avalanche, when more electrons (ions) are travelling towards the anode (cathode)(see fig. 2.1). Starting with one free electron, N electrons will arrive at the anode and (N-1) ions at the cathode.
Considering a concentration of n_0 electrons at the cathode, the electron density n at a distance x is determined by the ionization coefficient α according to:

$$dn \;=\; n(x)\;\alpha\;dx \tag{2.1}$$

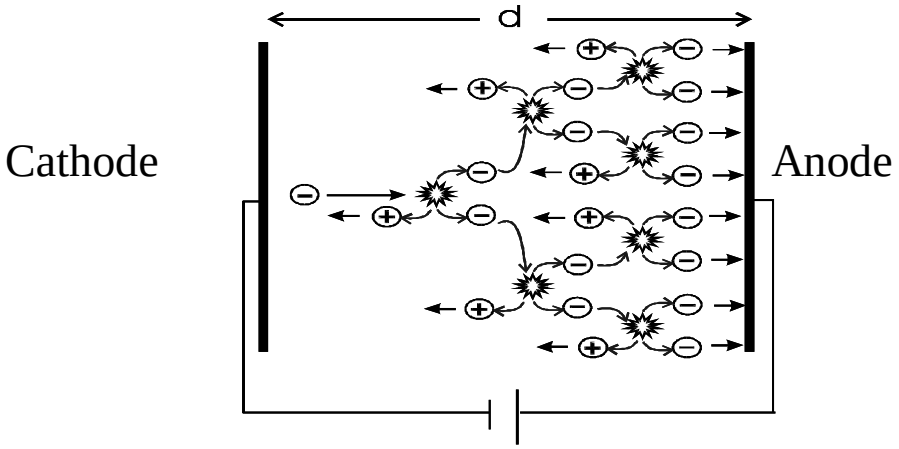

Figure 2.1: Schematic representation of the Townsend breakdown process.

where α is defined as the number of collisions per unit length that lead to ionization. Thus:

$$n \;=\; n_0 \; e^{\alpha x} \tag{2.2}$$

Assuming that all electrons eventually arrive at the anode, we find that $n_0 e^{\alpha d}$ electrons will arrive at the anode. As a result, the number of ions formed amounts to:

$$n_0 \; (e^{\alpha d} \;-\; 1)$$

These ions will move under the influence of the electric field to the cathode and there, as a result of collisions with the cathode release

$$\gamma \; n_0 \; (e^{\alpha d} \;-\; 1)$$

new electrons. γ is the secondary emission coefficient of the cathode. The value of γ depends on the cathode material, the type of gas and the energy of the ions, and is of the order of 10^{-2}. To achieve breakdown it is necessary that the amount of new electrons released is larger than the amount of electrons n_0 initially present at the cathode, leading to the following threshold:

$$\gamma \; (e^{\alpha d} \;-\; 1) \;\geq\; 1 \tag{2.3}$$

For a stable breakdown it is important that every electron yields on average one new electron in a collision with a gas atom, which leads to a discharge. The condition for an independent discharge is given in eq. 2.3 and is called the Townsend condition for breakdown, which can also be written as:

$$\alpha = \ln(1/\gamma + 1)/d \tag{2.4}$$

for flat electrodes at a distance d. Experimentally it is found that [2]:

$$\alpha = p * Ae^{(-B*p/E)} \tag{2.5}$$

in which p is the pressure, E the electric field, and A and B are constants which are determined by the gas. Rewriting both equations yields the following expression for the field strength E where breakdown occurs:

$$E = B * p/\ln(\ln(1/\gamma + 1)/(p * d * A)) \tag{2.6}$$

The expression for the minimum required breakdown voltage V_b in a homogeneous electric field, with electrode spacing d is found to be:

$$V_b = B * p * d/\ln(\ln(1/\gamma + 1)/(p * d * A)) \tag{2.7}$$

Because the secondary emission constant γ does not depend on E/p, we can express V_b as a function of p and the electrode spacing d:

$$V_b = f(p * d) \tag{2.8}$$

Plotting the breakdown voltage (V_b) of a certain type of gas as a function of p*d on a double logarithmic scale gives a so-called Paschen curve (fig. 2.2). Paschen curves are always positive parabolas, which is caused by the fact that at low pressures V_b is high because the electrons/ions have a small probability to hit a neutral atom whereas at high pressures V_b is high because the electrons/ions do not gain enough energy between the frequent collisions to ionize an atom. In the intermediate regime V_b has its minimum value.
The theory for Townsend discharge is found to be at least valid up to p*d=100 torr*cm, above the density of charged ions starts to play a role in the electric field profile. Under these conditions a description in terms of streamers can be more appropriate.
With the above equations it is possible to calculate the relevant properties

of N_2. N_2 in equilibrium at T = 300 K has typically it n= 100 cm^{-3} [15] free electrons. The mean free path is 1.5 10^{-4} cm at 600 torr and 4.4 10^{-4} cm at 200 torr. Using these values it is possible to calculate the speed of the electrons for the electric fields we mostly use in our experiments (40 kV, 15 mm), which is 6.8 10^6 m/s for 200 torr and 3.9 10^6 m/s for 600 torr. Officially the unit for pressure is Pa, but in gas discharge physics still torr is used, so we will keep using torrs in this thesis.
With equation 2.5 it is possible to calculate the Townsend ionization coefficients for a specific gas when A and B are known. Using A and B for N_2 from ref [16], results in:

$$\frac{\alpha}{p} = 5.0819 \exp\left(\frac{-268.81}{\frac{E}{p}}\right) \qquad 36.3 < \frac{E}{p} < 74.07 \ \mathrm{V} * \mathrm{cm}^{-1} * \mathrm{Torr}^{-1} \tag{2.9}$$

$$\frac{\alpha}{p} = 10.335 \exp\left(\frac{-312.042}{\frac{E}{p}}\right) \qquad \frac{E}{p} > 74.07 \ \mathrm{V} * \mathrm{cm}^{-1} * \mathrm{Torr}^{-1} \tag{2.10}$$

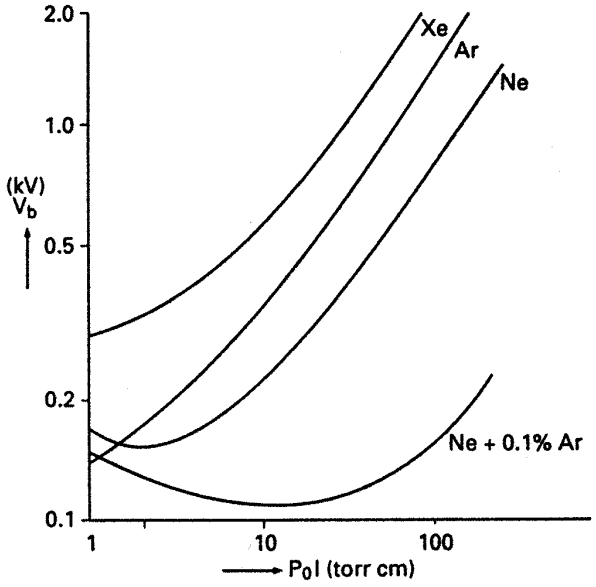

Figure 2.2: Paschen curves for typical gases: xenon, argon, neon and a mixture of neon + 0.1% argon [2].

Typical values of the Townsend ionization coefficient are, α=7.2 collisions/cm at 600 torr and 200 collisions/cm at 200 torr, expressing the fact that at 600 torr less collisions cause ionization and it is more difficult to start a discharge as compared to 200 torr.

2.1.2 Streamers

At values of $p*d > 100$ torr*cm and high electric fields, the simple description of Townsend is not appropriate anymore. At those high values the charge multiplication becomes so high that the space-charge field becomes comparable to the applied field, which occurs when the avalanche contains about 10^8 electrons [17]. The typical electron density is based on the following assumption. Consider a space charge of N ions contained in a spherical volume of radius r_0 at the streamer tip. The propagation condition is that a primary electron at an initial distance r_1 from the center of this sphere creates N ion pairs in an avalanche of diffusion radius r_0. The electric field can be calculated as follows:

$$E(r_1) \quad = \quad \frac{Ne}{4\pi\varepsilon_0 r_1^2} \tag{2.11}$$

Experimentally ≈ 31.4 kV cm^{-1} is found to be necessary for breakdown in a gap of 1 cm at 760 torr. Therefore N will be in the order of 10^8 to 10^{11} depending on the curvature at the tip which is typically between 10^{-2} and 10^{-1} cm.
The streamer transfers part of the potential of the electrode to its tip and the electric field ahead of the streamer tip is determined by the combined effect of the tip potential and the charged ion distribution. Streamers can be either cathode-directed (positive) or anode-directed (negative).
Eventually the formed streamers evolve into a very long highly conducting ionized channels, the tip of which has approximately the same potential as the electrode. The high temperature in the channel is responsible for a conducting, neutral (equal density of positive and negative charges) plasma. The very small voltage drop across the channel is due to the current flowing from the electrode to the tip.
The full development of a discharge in time as well as in space, can therefore be characterized by several typical temporal phases, shown in fig.

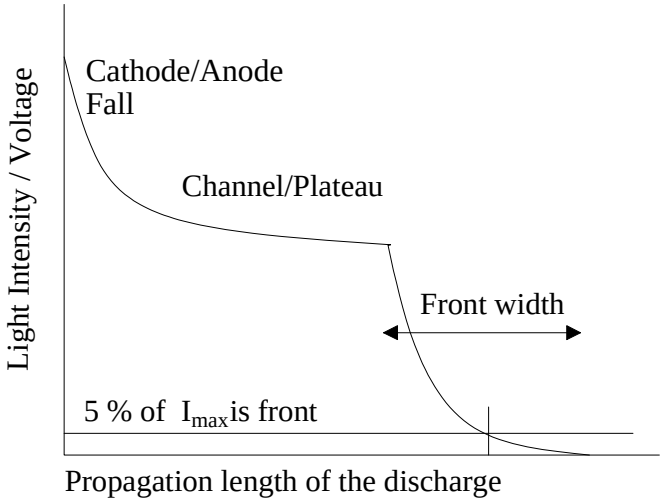

Figure 2.3: A schematic drawing of the profile of a discharge.

2.3 [9]. At the electrode there is a sharp drop of the potential (the anode/cathode fall) followed by the channel that transfers the electrode potential to the tip. At the tip the voltage again drops rapidly, accompanied by a strong electric field that ionizes the gas in front of it (streamer) enabling the discharge to propagate. Because the main issue of the thesis addresses the formation and propagation of streamers, the next section discusses it in more detail.

2.1.3 Formation and propagation of streamers

There are two possibilities for creating a streamer. One is that a sufficient ionization density is present at the beginning of the experiment. The other is that initial avalanches have to multiply until sufficient space charge is generated and the avalanche-to-streamer transitions occurs. In our case the second possibility looks more promising.
After the initial avalanche phase, the development of the streamer starts with the accumulation of a positive space charge close to the anode, caused by quasi immobile positive ions left behind by electron avalanches that either have been drawn towards the anode (for positive streamers), or that have been accelerated away from the cathode (for negative streamers) (see

fig 2.4). After this initial formation phase of the streamer it propagates by continuously ionizing the gas ahead of its tip. The difference between negative and positive streamers is the difference in propagation mechanism. In both cases the motion of the positive ions can be neglected during the streamer growth. The negative streamer tip is formed out of highly mobile electrons which have the tendency to diffuse out of the tip. The drift direction of the electrons is in the same direction as the propagation of the tip (see fig. 2.4).
Because for negative streamers the electrons ahead of the streamer tip move away from the tip, the electric field is falling more rapidly in directions perpendicular to the axis of the streamer. Therefore only electron avalanches which develop in the (tangential) direction of the streamer channel axis supply a significant ion charge to the streamer and more radially directed avalanches are less important. The opposite is true for positive streamers for which electrons are attracted to the higher electric

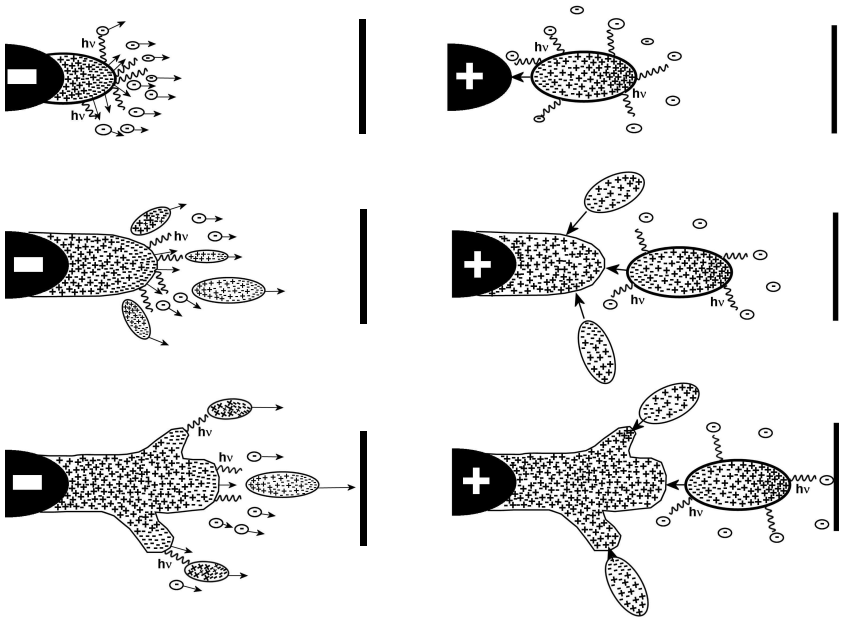

Figure 2.4: A schematic illustration of the propagation of a negative (left) and positive streamer (right) in an overvolted gap.

field in the tip region and the tip propagation is opposite to the electron motion (see fig. 2.4).
In this thesis we are primarily concerned with the streamer front and the way the gas is transformed from insulator to conductor. Here we deal with a highly non-linear phenomenon where space charge, generation and currents are strongly coupled and highly non-linear. Theoretically the basic equations that need to be solved are [11-14]:

- the balance equations:

$$\partial_t n_e \ + \ \nabla_{\mathbf{R}} \ \cdot \ \mathbf{j}_e \ = \ \mid n_e \mu_e E \mid \alpha_0 e^{-E_0/|E|} \tag{2.12}$$

$$\partial_t n_+ \ + \ \nabla_{\mathbf{R}} \ \cdot \ \mathbf{j}_+ \ = \ \mid n_e \mu_e E \mid \alpha_0 e^{-E_0/|E|} \tag{2.13}$$

  In which n_e and n_+ are the electron and ion densities respectively , and E is the electric field. The right hand terms describe the impact ionization of the gas molecules given by the product of the electron drift velocity $|v_e| = |\mu_e E|$, the electron density and the ionization coefficient α (eq 2.9 and 2.10).

- the Poisson equation:

$$\nabla_{\mathbf{R}} \ \cdot \ E \ = \ \frac{e}{\epsilon_0}(n_+ \ - \ n_e) \tag{2.14}$$

  which calculates the local electric field due to the local electron and ion concentrations.

- the electron and ion current densities $\mathbf{j}_e$ and $\mathbf{j}_+$:

$$\mathbf{j}_e \ = \ -n_e \mu_e E \ - \ D_e \nabla_{\mathbf{R}} n_e, \quad \mathbf{j}_+ \ = \ 0 \tag{2.15}$$

  where $\mathbf{j}_e$ is the sum of a drift and a diffusion term. The ion current $\mathbf{j}_+$ is neglected, since ions are much less mobile than electrons.
  All relevant quantities are position and time dependent.

It is a matter of controversy [18] whether photoionization plays an important role. In this case, photogeneration should be included in the balance equation (eq. 2.12) i.e. an extra source term of electrons. If photoionization takes place in the vicinity of the primary avalanche, the secondary avalanches, produced by the photon create free or weakly

bound electrons, which may intermix with the primary ions and play a role in forming a quasi-neutral plasma. Furthermore, this process can be reinforced when molecules that are excited emit photons that ionize other molecules.
It is important to notice that the streamer growth is not only limited by the rate of ionization in front (by avalanche production or by direct impact ionizations) but also by the rate of neutralization of the positive charge behind the tip, which is basically determined by the electron drift velocity.
The propagation velocity of the streamer is very rapid (in the order of 10^8 cm/s) which is much faster than the drift velocity of the electrons in the external field necessary for breakdown (at most 10^7 cm/s). Some authors [19, 20] have considered this very rapid propagation (1% of the speed of light) as a strong indication that photoionization plays an important role. Others [11-14] consider the ionization front at the tip of the discharge as an ionization 'shock front' of a few micrometers thickness.

2.2 Open questions

An important question which was pointed out may years ago and is still not answered, is the actual role of the streamer channel during propagation. Basically two models have been put forward in history and are discussed nowadays by many people [2,21] :
1) Dawson and Winn [22] have worked out a model which Raether [5] already described namely that the streamer head can be described as a propagating isolated sphere of positive space charge, living on the expense of its own potential energy, which has been accumulated in the high electric field near the point electrode in the early stage of the breakdown. In this description the channel behind the tip plays only a minor, passive role.
This model has been considerably improved by Gallimberti [8], who took into account the energy balance of processes involving the external field. He found that the streamer needed a background electric field of about 7 kV/cm for a stable propagation to account for the loss of energy due to inelastic collisions between the electrons and molecules. A stability field

of 4.5 - 5 kV/cm has actually been observed in long gaps [23].
2) Wright [24] and Klingbeil *et al* [25] have proposed a model where the streamer channel is strongly conducting, "transmitting"the electrode potential to the tip and thus playing a major role for the streamer propagation. So far unambiguous evidence in favor of one of the models is absent, and experiments and numerical calculations [11] suggest that the reality lies somewhere in between. As we will see our results also lead to this conclusion.
The main issue of this thesis is to verify experimentally whether the predictions of various numerical calculations provide a realistic description of the streamer propagation [11-14]. A particular outcome of some of these calculations is that the negative streamer propagates as a thin charged ionization sheet with a width of only a few μm. As a specific example we reproduce the outcome of the numerical calculation by Vitello et al. in fig. 2.5. The evolution of the electron density between two planar electrodes, 5 mm apart, is plotted at three different times after formation. Each contour line depicts one order of magnitude change in the density. The streamer propagates as a fingerlike region, containing a nonequilibrium

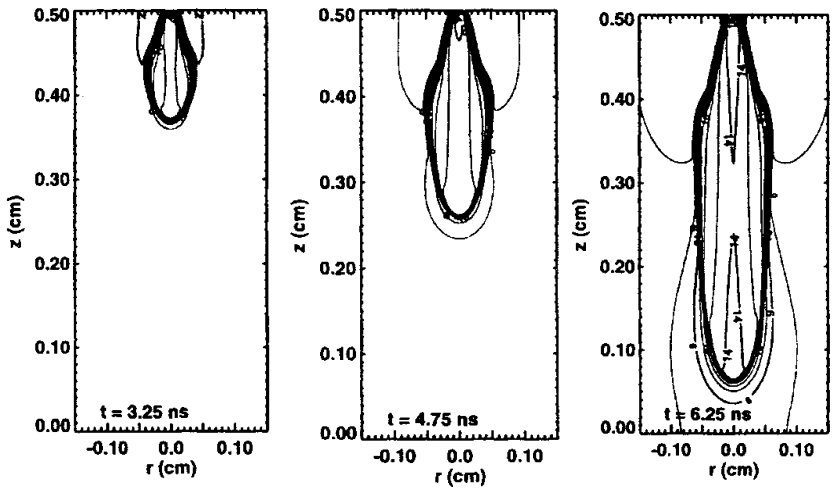

Figure 2.5: Electron density profile in a negative streamer (-30 kV at 760 Torr in nitrogen) from the 3D cylinder-symmetric numerical simulations of P.A. Vitello [12].

plasma and surrounded by a nonionized gas. The transition from plasma within the streamer to normal gas outside occurs within a few micrometers and exhibits a change of electron density of about 10^{10} times. Apart from testing whether the width of the ionization sheet indeed is as narrow as a few micrometer, our experiment will determine other parameters, such as the radius of the streamer tip, the velocity of the wavefront, the field enhancement near the tip, the propagation of the tip and the shape/building up of the tip. Until recently such experimental information has not been available, mainly because the experimental conditions under which the discharges are formed are very demanding to systematically investigate the streamer formation and propagation. Firstly, the full development of the streamer and its subsequent propagation only takes a few nanoseconds. Secondly, due to the highly non-linear nature of discharges, no two discharges are alike. Finally, it is very difficult to perform a reliable measurement without disturbing the discharge. Only after the recent advent of sufficiently fast electronics together with sophisticated intensified fast CCD cameras it has become possible to generate discharges in a relatively controllable way, to follow the accompanying electrical transient and simultaneously image the time-resolved emission in order to visualize the streamer propagation.

2.3 Bibliography

[1] Coulomb, *Mémoires de l'Académie des Scienes*, 1785 p612.

[2] Yu. R. Raizer, *Gas discharge physics*, Springer-Verlag, Berlin, New York 1991.

[3] J.S. Towsend, *The theory of ionization of Gases*, Constable, London, 1910.

[4] J.M. Meek, Phys. Rev. **57** (1940), 722

[5] H. Raether, Arch. Elektrotech, **34** (1940), 49. H. Raether, Phys. Z. **112** (1939), 464 [in German].

[6] L.B. Loeb, *Basic Process of Gaseous Electronics*, University of California Press, Berkeley CA 1960

[7] E. Marode. J. Appl. Phys. **46** (1975), 2005 and in *Electrical Breakdown and Discharges in Gases*, ed. by E.E. Kunhardt and L.H. Luessen, NATO ASI Series B **89B** (Plenum Press, N.Y. and London, 1983). 119*ff*

[8] I. Gallimberti, J. Physique **40** (1979), C7-193 and in *Electrical Breakdown and Discharges in Gases*, ed. by E.E. Kunhardt and L.H. Luessen, NATO ASI Series B **89A** (Plenum Press, N.Y. and London, 1983). 265*ff*

[9] S. Larigaldie, J. Appl. Phys. **61** (1987) 90*ff* and 102*ff*

[10] K.P. Uhlig, Surface discharges (Lichtenberg figures) in high magnetic fields, Ph.D. thesis, Universität Konstanz (1991).

[11] S.K. Dhali and P.f. Williams, Phys. Rev. A **31**, 1219 (1985); and J. Appl. Phys. **62**, 4696 (1987).

[12] P.A. Vitello, B.M. Penetrante, and J.N. Bardsley, Phys Rev. E **49**, 5574 (1994).

[13] U. Ebert, W. van Saarloos and C. Caroli, Phys. Rev. Lett **77**, 4178 (1996); and Phys. Rev E **55**, 1530 (1997).

[14] Manuel Arrayás, Ute Ebert, and Willem Hundsdorfer, Phys. Rev. Lett. **88** (2002), 174502.

[15] W.F.L.M. Houben *Pulsed corona-Induced degradation of organic materials in water*, thesis University of Eindhoven, 2000.

[16] J.T. Kennedy *Study of the avalanche to streamer transition in insulating gases*, thesis University of Eindhoven, 1995.

[17] L.B. Loeb and J.M. Meek, J Appl. Phys. **11** (1940), 438.

[18] U. Ebert, W. Hundsdorfer, Phys. Rev. Lett. **89** (2002), 229402.

[19] A.A. Kulikovsky, J. Phys. D, Appl. Phys. **33** (2000), 1514.

[20] S.V. Pancheshnyi, S.M. Starikovskaia, and A. Yu Starikovskii, J. Phys. D, Appl. Phys. **34** (2001), 105.

[21] E.M. Baxelyan and Yu. R. Raizer, *Spark discharge*, CRC Press, Berlin, New York 1998.

[22] G.A. Dawson and W.P. Winn, Z. Phys. **183** (1965), 159

[23] R.F. Griffiths and C.T. Phelps, Quart. J. R. Mat. Soc. **102** (1976), 419

[24] J.K. Wright, Proc. Roy. Soc. London, **A 280** (1964), 23

[25] R. Klingbeil, D.A. Tidman, and R.F. Fernsler, Phys. fluids **15** (1972), 1969

Chapter 3

Experimental details

Introduction

Discharges are very rapid phenomena with propagation velocities approaching 1 % of the speed of light. Furthermore, streamers are very non-linear phenomena and therefore very difficult to reproducible, where each new streamer is different from the previous one, not only regarding the shape but also the development in time. Nevertheless many characteristics of streamers like their dependence on voltage, gas pressure, electrode topology etc. are actually common to all streamers measured under similar conditions. The very nature of streamers makes it almost impossible to perform non-invasive experiments other than optical observation, which is practically the only non-perturbative technique that can be used. As we will discuss later the measurement of the emitted light caused by a discharge allows important observations. Unfortunately the experiment gives only indirect information on relevant quantities as the local charge densities, the local conductivity and the local electric field. Nevertheless nowadays the emitted light can be measured with sufficiently fast time resolution, simultaneously with the resistivity of the gas, which provides a very powerful non-invasive measurement technique. Fig. 3.1 shows the set-up which has been used to study the growing of a free gas discharge. This type of discharge is different from Lichtenberg figures [1, 2], where a gas discharge propagates along the surface of an

insulating plate, that separates two electrodes from each other. The advantage of a free discharge is, that there is no interaction between the discharge and the insulating plate, and that purely the evolution of the spark in the gas is measured. As a consequence the number of unknown parameters is minimized. Another important aspect of this work is that the growth of the discharge is studied with a fast Intensified CCD camera, which enables the first real observation of how and where the gas is transformed from insulator to conductor in real time.
There are two crucial elements for the success of our experiment, first to make reproducible high voltage pulses (HV pulses), second to measure image, voltage and current simultaneously on a nanosecond scale. Because only one image per spark can be made with a time resolution of about 0.1 nsec, it is very important that every high voltage pulse is the same, especially the risetime, in order to be able to compare different sparks. To study the growth of the discharge we need approximately 100 snapshots of sparks at different delay times. Therefore it is also very important to know the exact time (with less than a nanosecond resolution) at which the spark starts.
This chapter describes the circuit used to generate high voltage pulses (3.1) and how current and voltage are measured (3.2). The discharge chamber is discussed in 3.3, whereas the synchronization of the optical gated observation with the electrical signals is described in 3.4. An analysis of the relation between the emitted light and the characteristics of the spark is described in 3.5.

3.1 Generation of high voltage pulses

The technology to make high voltage pulses has been described in many textbooks [3]. In our case the situation is slightly more complicated because we use the HV pulse to generate a discharge. The discharge represents a load resistance on the source which has both capacitive and resistive components, that vary enormously with time as the spark develops. Usually, high voltage pulses with a risetime of a few nanoseconds can be obtained with a spark gap as HV switch. Such a design has a high inductance, which is not convenient here because of the varying load.

Instead a linefeed generator is used as a source, where a coaxial line of a certain length is charged and then switched using a spark gap. The resulting pulse, the length of which is determined by the length of the charged cable, travels along a coaxial line which ends at the discharge chamber. In the coaxial line the capacity and the inductance are distributed over the whole length of the line and are given by:

$$C = \frac{1}{v_p Z_0} \qquad\qquad L = \frac{Z_0}{v_p} \tag{3.1}$$

where v_p is the phase velocity and Z_0 is the characteristic impedance. The home built generator is shown in fig. 3.1. The transmission line T_1 (Z_0 = 50 Ω) represents the capacitor and is charged by a powersupply (P.S.) via R to voltage V_0. The spark gap S_1 is non-conducting as long as the

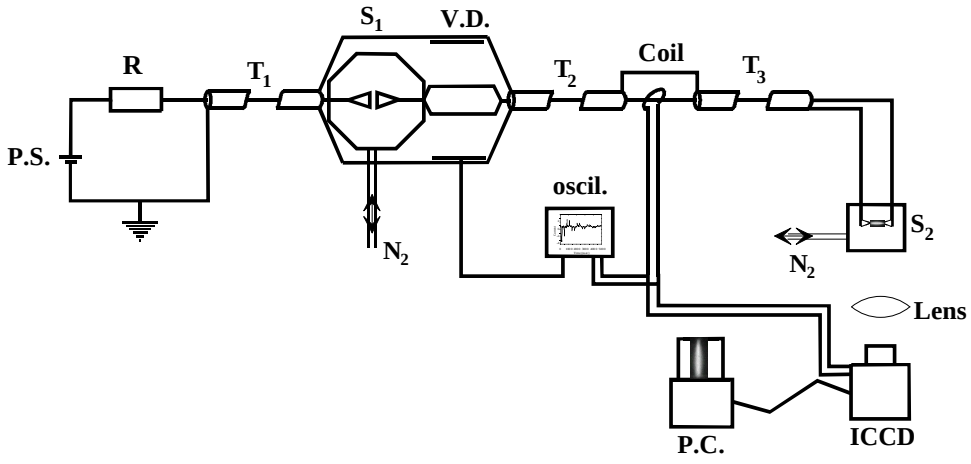

Figure 3.1: Schematic representation of the set-up, consisting of a powersupply (P.S.) which loads transmission line T_1, a spark gap S_1 which feeds a high voltage pulse onto transmission lines T_2 and T_3 towards the actual discharge chamber S_2 filled with nitrogen gas. The electrical transients are measured using a voltage divider (V.D.) and a coil (incoming pulse) and a fast oscilloscope. The light emission of the discharge is imaged on a gated ICCD camera.

pressure of the nitrogen gas inside the spark chamber is high enough to prevent breakdown between the electrodes. S_1 is triggered by relieving the pressure instantaneously, which leads to a rectangularly shaped HV pulse of amplitude $V_0/2$, which is fed into the second transmission line T_2, leading to the actual discharge chamber.
The spark gap S_1 has a large coaxial geometry in order to match the impedance of the transmission line and to keep the reflections at a minimum. The shape of the HV pulse is measured with a capacitive voltage divider (V.D.) included into the coaxial set-up and with a current transducer (coil). The charging resistor R (170 MΩ) is chosen to make the charging time of T_1 much longer than the pulse length, giving pulses with a flat top.
The operation principle of the generator can be understood from the following scheme (fig. 3.2). When S_1 is open there is a voltage V_0 over the line, which can formally be described as two waves of amplitude $V_0/2$, travelling in opposite directions. At the closing of S_1 the impedance at the end of T_1 will rapidly go from infinity to 50 Ω, the designed impedance of the spark gap. Since the spark gap is switched very quickly, a rectangular pulse with amplitude $V_0/2$ moves along the impedance matched (50 Ω)

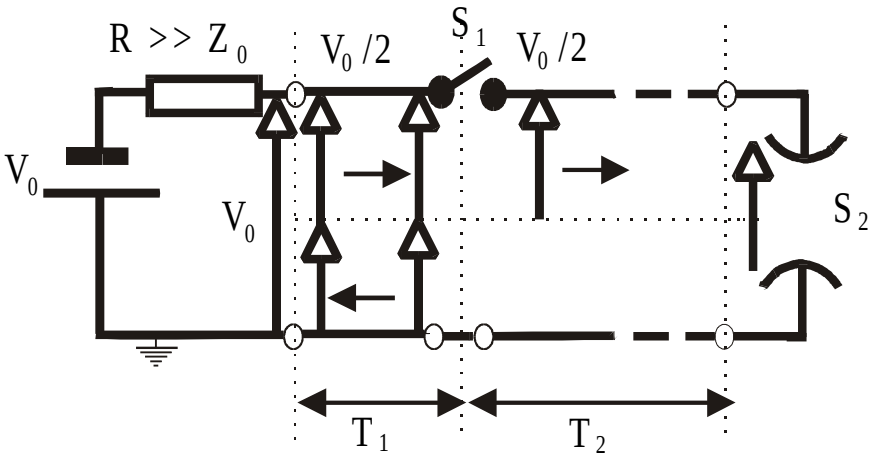

Figure 3.2: Equivalent wave representation of the linefeed generator.

transmission line T_2, towards the actual spark chamber S_2. In this case, the length of the HV pulse Δ is given by :

$$\Delta = \frac{2\ell}{v_p} \tag{3.2}$$

where ℓ is the length of the transmission line (T_1) and v_p the phase velocity. Our transmission line, a line of 10 m, produces a pulse of 200 nsec with a risetime (10% - 90%) less than 10 nsec. To vary the duration of the pulse, the length of transmission line T_1 can be changed.

3.2 Analysis of the electrical transients

In order to measure the output HV pulse, a capacitive voltage divider has been incorporated in the coaxial arrangement that also contains the spark gap S_1 (fig. 3.1). Furthermore a current probe has been built in, halfway the transmission line (T_2), to measure the shape and amplitude of the current pulse.
The design and the theory of a capacitive voltage divider has been explained by many authors (see e.g. [2, 4, 5]), and is realized as shown in fig. 3.3. The divider is formed by a 20 cm long, 60 μm thick Kapton cylinder, coated on one-side by aluminium. The divider ratio is determined by the ratio of the capacity C_1, between the inner conductor of the

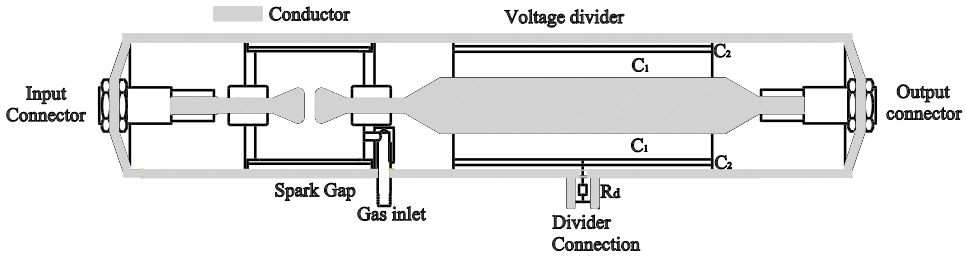

Figure 3.3: Overall drawing of the trigger unit with the capacitive voltage divider.

tube and the Al coating, and the capacity C_2, between the Al coating and the coaxial housing of the tube. With our dimensions a divider ratio of 440 is obtained. The decay time of the response is given by the following equation:

$$\tau_{dec} = (R_d + Z_{osc}) \cdot C_2 \cdot \ell_d \tag{3.3}$$

in which R_d is the resistor (220 Ω) included in the divider (fig. 3.3), Z_{osc} is the input impedance of the oscilloscope and ℓ_d the length of the divider. With a length of 20 cm, $\tau_{dec} \cong 450$ nsec, which is sufficiently long to measure pulses of about 200 nsec.
Current measurements need a current sensor with a broad frequency response, and these are commercially available as current transducers (Rogowski probes). The probe employs the principle that a current flowing in an electrical circuit produces a magnetic flux proportional to the current. This magnetic flux is picked up via the ferrite core of the current transducer and the induced flux is measured by a second coil around the ferrite. The risetime of the current transducer is 3 nsec.
With the voltage divider and the current transducer not only the pulse can be measured but also the reflections coming back from the gas discharge (see fig. 3.1). From the shape of the reflection it is possible to determine with high accuracy (within less than a nsec.) when the discharge has started. Using this measurement, the time at which the ICCD camera has made the image with respect to the beginning of the spark can be determined, as will be explained later.

3.3 The discharge chamber

To study discharges many types of geometries can be used. The optimal choice of a certain type of geometry depends on which parameters of the discharge one wants to study. Three different configurations are shown in fig. 3.4. In the wire-cylinder geometry (fig. 3.4b) the electric field distribution is the most simple one, because it depends only on the radial distance. Therefore the maximum number of streamers and the energy density per unit volume is higher than in the point-plate configuration (fig. 3.4a) [6]. These aspects make the wire-cylinder geometry the most suitable for gas cleaning. It is however very difficult to follow the formation and propagation of streamers, especially when a large number

of streamers are produced and it is not possible to distinguish them. In the wire-plate geometry (fig. 3.4c) this problem is solved, although still many streamers can start simultaneously and it is impossible to measure the current in each individual streamer. In addition, the streamers also may interact with each other. The best geometry to image the formation and propagation of streamers is the point-plate configuration (fig. 3.4a), where only one streamer starts at a time under suitable conditions. Furthermore, most theoretical calculations have been performed for similar configurations [7].
In fig. 3.5 a schematic drawing of the discharge chamber is given. Since the available space inside a high field Bitter magnet is limited the distance between the two electrodes must be restricted to 15 mm. The chamber can be evacuated down to a pressure of 1 torr and allows for easy changing of the gases inside. The electrodes have been made of stainless steal and have been fixed in such a way that they can be changed very easily, allowing to measure different geometries. It is not necessary to match the impedance of the spark chamber to the 50 Ω of the cables, because its impedance anyway varies from quasi infinite to very low values during breakdown. As a consequence, the incoming voltage pulse will be partially reflected.

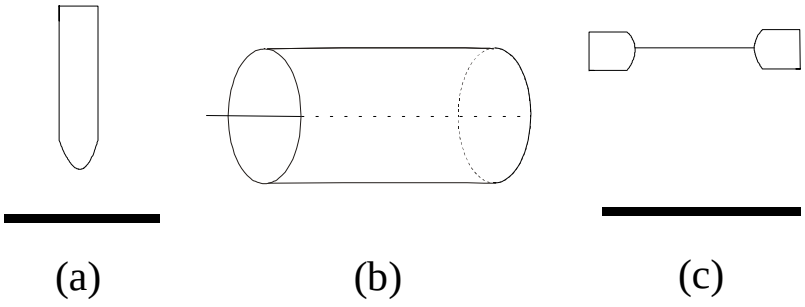

Figure 3.4: Discharge configurations, (a) point-plate, (b) wire-cylinder, (c) wire-plate.

Before every measurement series (all measurements at one voltage or at one pressure) the electrodes were carefully cleaned to avoid effects of oxidation. The position of the point and plate electrodes was measured from a white light image, as shown in fig 3.6. The high voltage (positive or negative) pulse was always applied to the point electrode. Before the actual measurements start, after cleaning the electrode, the current pulses of at least 50 discharges are measured after which the reflections are found to be the same for every discharge.

3.4 Timing and optical measuring of the discharge

Timing is very crucial in our experiment, because the intensified CCD camera can only take one image of 5 nanoseconds length per millisecond and can therefore only make one snapshot of each discharge. The intensifier of the CCD is gated by an electronic shutter. This shutter action

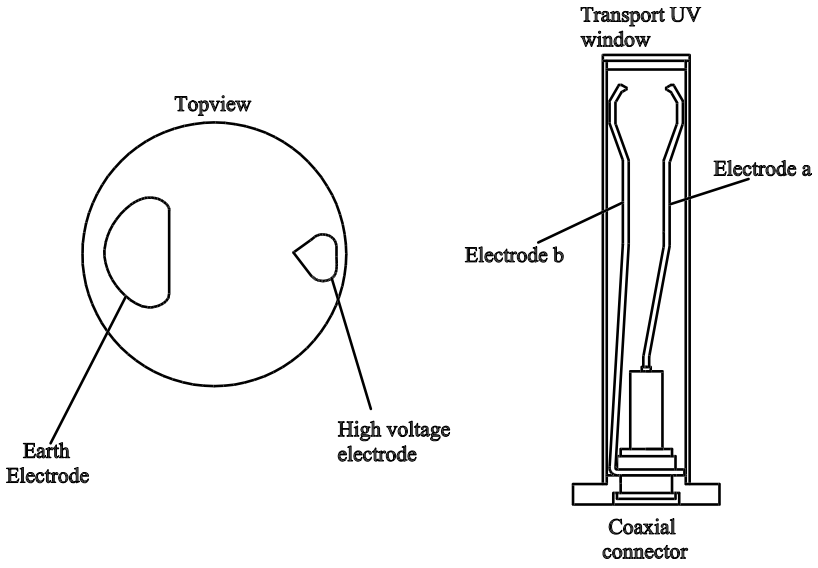

Figure 3.5: Schematic drawing of the discharge chamber.

is produced by controlling the photocathode of the image intensifier, and can be varied from 5 nsec. up to seconds. The electronic shutter on/off ratio is very high, 5×10^6 and therefore this camera is very suitable to measure low intensities and events which only have a duration of a few nsec.
To study the propagation, different sparks at different delay times should be imaged. The actual delay time of the measured image is determined from simultaneously recorded electrical signals of the discharge. Fig 3.7 schematically displays the signal of the current transducer, the voltage across the discharge chamber, the trigger signal and the electronic shutter

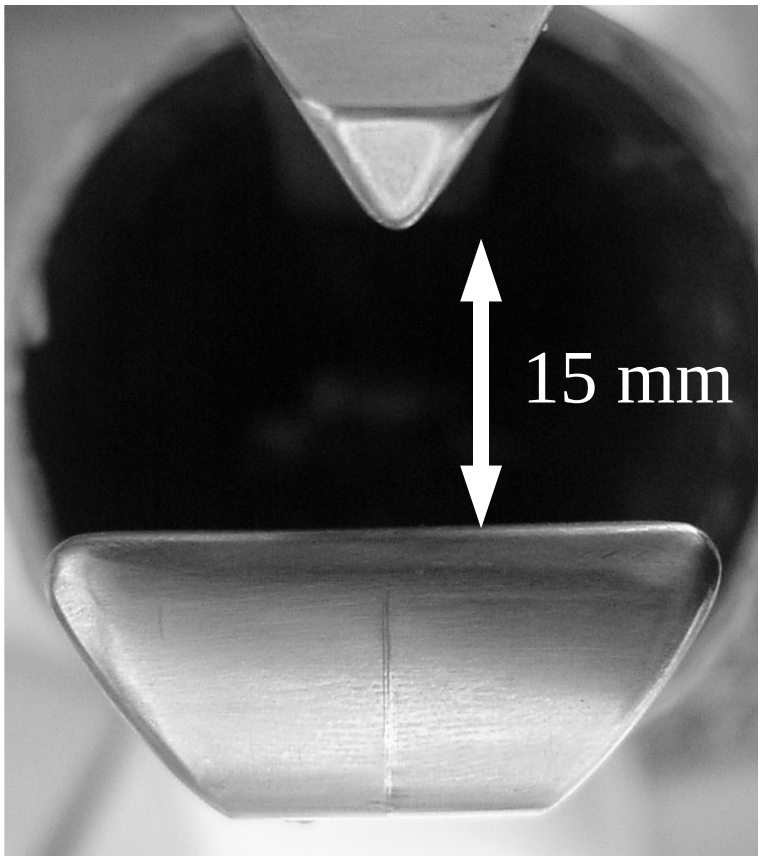

Figure 3.6: White light photograph of the electrodes. At the top the point electrode and at the bottom the plate electrode.

of the camera. At t= 0 the HV pulse from the line feed generator reaches the current transducer in between transmission lines T_2 and T_3 (fig. 3.1). This pulse arrives at t = 125 nsec. (the lengths of T_2 and T_3 equal half the length of T_1) at the electrodes and lasts 250 nsec. (corresponding to the line feed length of T_1). When the pulse does not generate a spark it

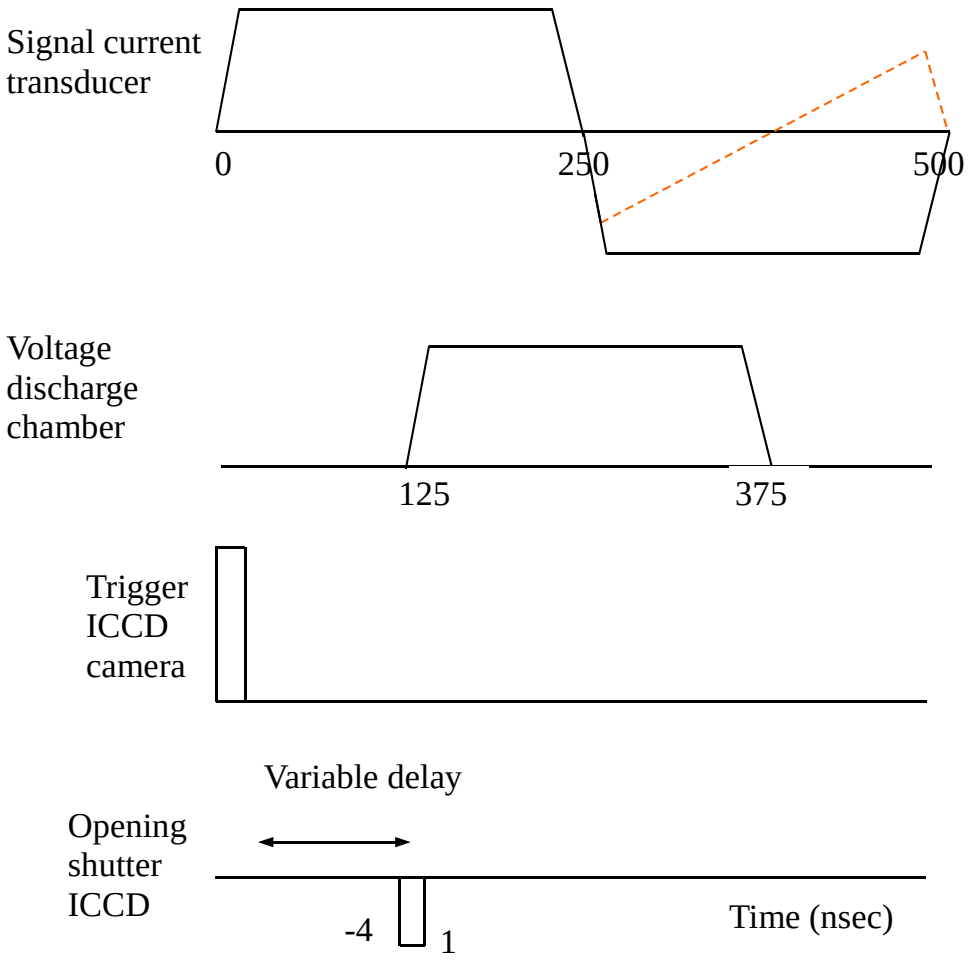

Figure 3.7: Typical triggering scheme of the ICCD camera. The 250 nsec wide square-like HV pulse arrives at the discharge chamber at about 125 nsec. By properly setting the delay of the electronic shutter of the ICCD camera the onset of the streamer formation can be monitored.

is reflected back and arrives as a negative signal at the current transducer after 250 nsec (solid line in top panel fig. 3.7). When a spark is initiated, the changed impedance of the discharge chamber leads to a different reflected signal (dashed line). The precise initiation time of the spark is given by that moment when the reflected signal starts to deviate from the reflection measured without spark production i.e. for infinite resistance.
The ICCD camera is triggered by a signal from the current transducer, on the ongoing flank of a HV pulse, 125 nsec. prior to the arrival of the pulse at the discharge chamber. The shutter of the camera is opened during 5 nsec. with an adjustable delay (of nsec precision) after the triggering of the camera. The bottom panel of fig. 3.7 depicts a typical triggering scheme. The shutter of the camera opens 4 nsec. before the arrival of the HV pulse, and remains open for 5 nsec, which means that in this case the image corresponds to a time integrated image of the first nanosecond after the arrival of the pulse. By using this method it is possible to image the rapidly propagating pulse, with a gate time of 5 nsec. that is larger than the typical streamer formation. The precise timing of the snapshot is determined afterwards. The exact moment the discharge starts is very difficult to predict due to its non-linear nature. Furthermore, a small electronic jitter is hard to avoid in the equipment, which implies that the moment the shutter opens might vary from pulse to pulse. However these two moments in time can be measured afterwards with a precision of 0.1 nsec. by looking at the change in the reflected pulse on the current transducer (i.e. the start of the discharge) and the triggering signal of the intensifier. A typical example is shown in fig. 3.8. The grey curve corresponds to the measured signal without a discharge. The black curve starts to deviate at a certain moment in time, which marks the onset of the spark. By comparing this time with the trigger signal of the ICCD camera the time delay can be determined accurately. By this method and by repeating the experiment several (typically 100) times, the time evolution of the spark can be reconstructed.
In the rest of the thesis time t=0 corresponds to the start of the discharge. Images are taken at a certain delay that is the time after the starting of the discharge.
The current transducer measures the height of the applied and reflected pulse of the discharge which makes it possible to calculate the impedance

of the discharge at every moment, using the following formula:

$$V_{\text{ref}} = V_{\text{pulse}} \frac{R_{\text{dis}} - Z_{\text{trans}}}{R_{\text{dis}} + Z_{\text{trans}}} \tag{3.4}$$

in which V_{ref} is the voltage of the reflected pulse, V_{pulse} is the voltage of the incident pulse, Z_{trans} is the impedance of the transmission line and R_{dis} is the impedance of the discharge. Therefore it is possible to determine the resistance of the discharge with the same time resolution as the resolution of the images (0.1 nsec.).

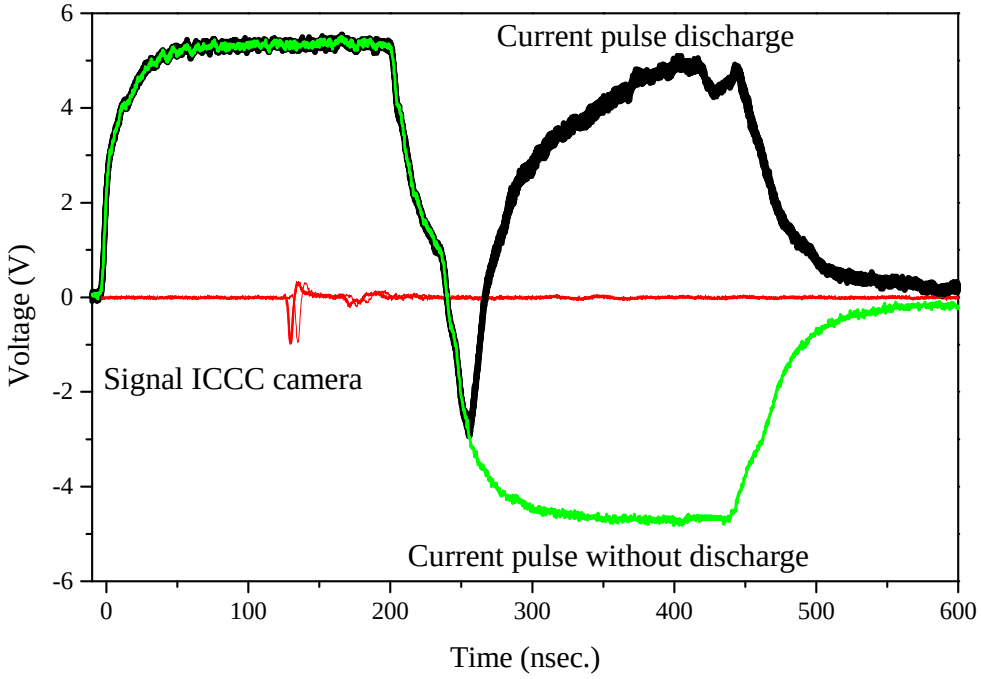

Figure 3.8: The HV current pulse with (the black curve) and without discharge (the grey curve). The moment in time where the black curve start to deviate marks the formation of a spark. The small pulses correspond to the signal of the intensifier of the ICCD camera, which enables a precise determination of the time-delay of every image.

3.5 Properties of N_2 discharge emission

The spectrum of a typical N_2 discharge has been measured from 200 nm until 1100 nm (fig. 3.9) using a fiber coupled optical spectrometer, with a resolution of 1 nm. It should be noted that the spectrum in fig. 3.9 corresponds to the time-integrated emission of the discharge, including the formation and propagation of the streamer as well as the channel. Since we are mainly interested in the streamer dynamics we use optical filters to isolate the streamer emission. To this end we make use of the fact that the streamer is cold and has a gas temperature only slightly above that of the surrounding air [8]. Under these conditions the electric field accelerates the electrons leading to excitation of N_2 molecules to the $N_2(C^3\Pi_u)$ and $N_2^+(B^2\Sigma_u^+)$ electronic states, which have roughly the same value of the internuclear distance as the ground state $N_2(X^1\Sigma_g^+)$ (see fig. 3.10).

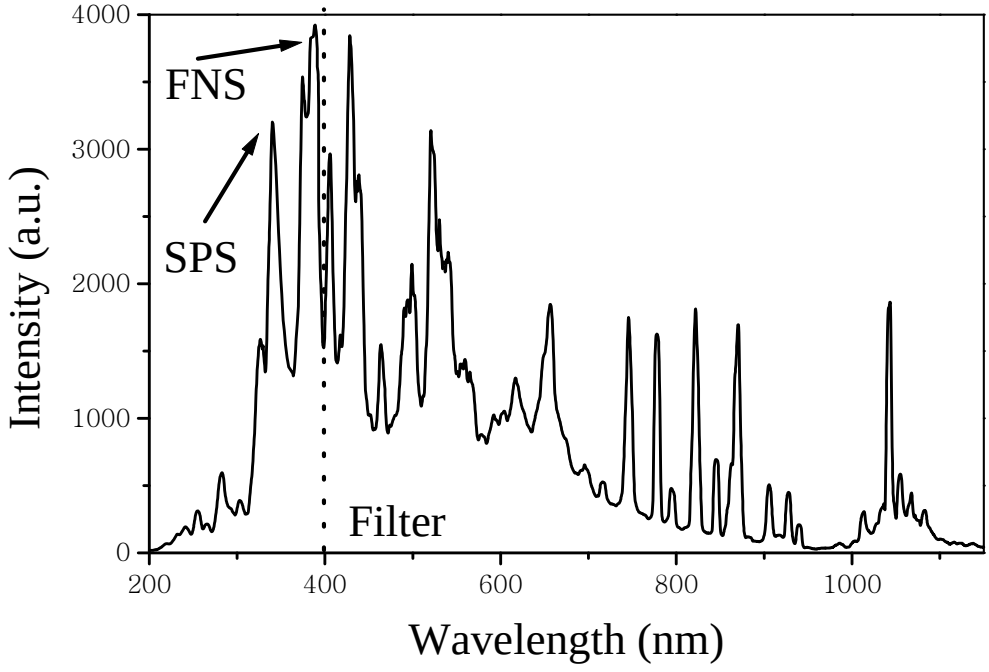

Figure 3.9: Measured emission spectrum of a nitrogen discharge.

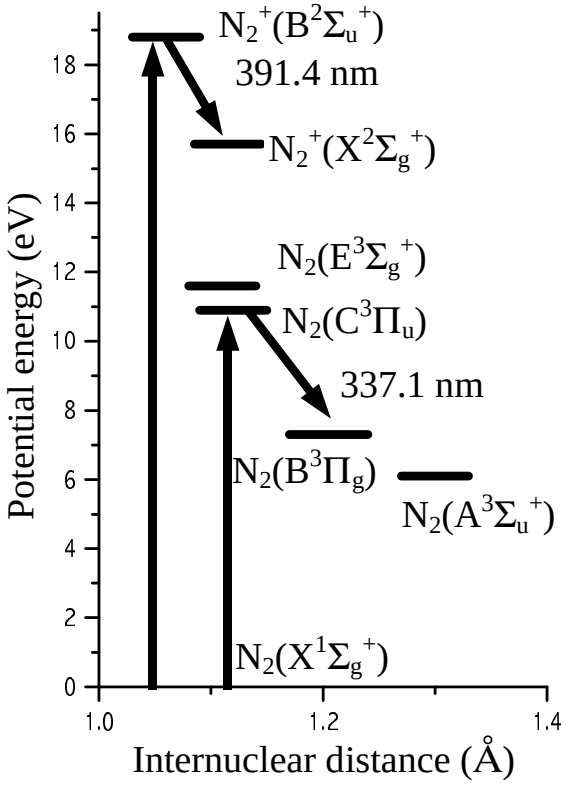

Figure 3.10: Part of the potential energy diagram of N_2 and N_2^+.

According to the Franck-Condon principle (high probability of transitions between states with similar internuclear distance), the following direct electron impact excitations are very likely:

$$N_2(X^1\Sigma_g^+)_{\nu=0} + e(>11.0eV) \rightarrow N_2\,(C^3\Pi_u\,)_{\nu'} + e$$

$$N_2(X^1\Sigma_g^+)_{\nu=0} + e(>18.7eV) \rightarrow N_2^+(B^2\Sigma_u^+)_{\nu'} + 2e$$

The ground state level has a large population at the experimental conditions of the streamer. The excited states relax due to spontaneous emission and molecular quenching effects [9, 10]. The most intense radiative transitions, are the Second Positive System (SPS) of N_2 and the First Negative System (FNS) of N_2^+; leading to the following emission

peaks:

$$SPS: \quad N_2\,(C^3\Pi_u\,)_{\nu'} \;\rightarrow\; N_2\,(B^3\Pi_g\,)_{\nu''} \quad \lambda(\nu' = 0, \nu'' = 0) \;= 337.1\,\text{nm}$$

$$FNS: \quad N_2^+(B^2\Sigma_u^+)_{\nu'} \;\rightarrow\; N_2^+(X^2\Sigma_g^+)_{\nu''} \quad \lambda(\nu' = 0, \nu'' = 0) \;= 391.4\,\text{nm}$$

These two transitions explain the bright peaks below 400 nm in fig. 3.9. The other peaks predominantly originate from other processes in the gas probably at later stages of the discharge. In order to exclude those peaks from the image we have positioned an optical low-pass filter in front of the ICCD camera which blocks all wavelengths above 400 nm. In some experiments we have also used bandpass filters centered around 337 nm (width 15 nm), to measure the FNS line or centered around 390 nm (width 10 nm), to measure the SPS line.
In the following we will implicitly assume that the intensity of the measured light is proportional to the number of ionized molecules. The underlying idea is that the number of excited states is proportional to the number of ionized molecules as a result of the distribution in energy of colliding electrons. Some electrons with a long mean free path are able to ionize, whereas others which collide earlier with a lesser kinetic energy will only excite neutral gas molecules. As long as there are no particular energies which ionize or excite more effectively than others, it is reasonable to assume that the electron distribution is reflected in the distribution of ionized and excited states of nitrogen.
A more severe drawback of equating the emitted light to the local density of ions is that the radiative lifetime of the excited N_2 states is on the order of a nanosecond. As a result emission will occur from molecules that have been excited a nanoseconds earlier. This finite radiation lifetime will therefore lead to an apparent fuzzyness of the images because the propagation velocity is so rapid. A hypothetical infinitely sharp ionization front will lead to a band of emitted light given by the product of propagation velocity times lifetime which in the worst case scenario is of the order of a few mm for the fastest propagating discharge (3 10^6 m/s), but usually much less than a mm. Therefore although we can achieve a better precision experimentally on the timing of the electronics and the images, there is an inherent error due to the finite lifetime.

3.6 Bibliography

[1] G.Ch. Lichtenberg, Novi Commentarii Societatis Regiae Scientiarium Gottingae tom **8** (1778), 168.

[2] K.P. Uhlig, Surface discharge (Lichtenberg figures) in high magnetic fields, Ph.D. thesis, Universität Konstanz (1991).

[3] F.B.A. Früngel, High speed pulse technology, (Acedemic Press, London, New York, 1.ed., 1965)

[4] F. Gygi and F. Schneider, report n$^{\underline{o}}$ 64-46 (Cern, Geneva, 1964), 8.

[5] A.J. Schwab, Hochspannungsmeßtechnik (Springer Verlag, Berlin, 1982), 73.

[6] Y.L.M. Creygthon, Pulsed positieve corona discharges, Ph. D. thesis Technische Universiteit Eindhoven (1994).

[7] P.A. Vitello, B.M. Penetrante, and J.N. Bardsley, Phys Rev E **49**, 5574 (1994).

[8] G. Hartmann, Spectroscopie de la décharge couronne: étude des méchanismes de collisions dans le dard (streamer), Ph.D. Thesis no. 1783, Université de Paris-Sud, Centre d´Orsay (1977).

[9] K.B. Mitchell, J. Chem. Phys. **53** (1970), 1775.

[10] J.M. Calo and R.C. Axtmann J. Chem. Phys. **54** (1971), 1332.

Chapter 4

General characteristics of negative and positive discharges in N_2

4.1 Introduction

In this chapter we will sketch the global evolution of a discharge in N_2 starting with the formation of a streamer and evolving into the fully grown spark closing the gap between the electrodes. Specific emphasis is on the initial stages of the discharge where the ionization front is build up. This ionization process and the topology of the streamer front is one of the most controversial issues of the discharge propagation and is theoretically described as a typical example of non-linear pattern formation. We will focus on describing the general appearance of the discharges, as measured by our time-resolved imaging technique.

4.2 Imaging of discharges

4.2.1 From avalanche to breakdown

Fig. 4.1 displays typical images of the emitted light of a N_2 discharge at different delay times, covering the whole evolution from avalanche to breakdown, for a negative discharge (-40 kV) at 200 Torr. In fig.

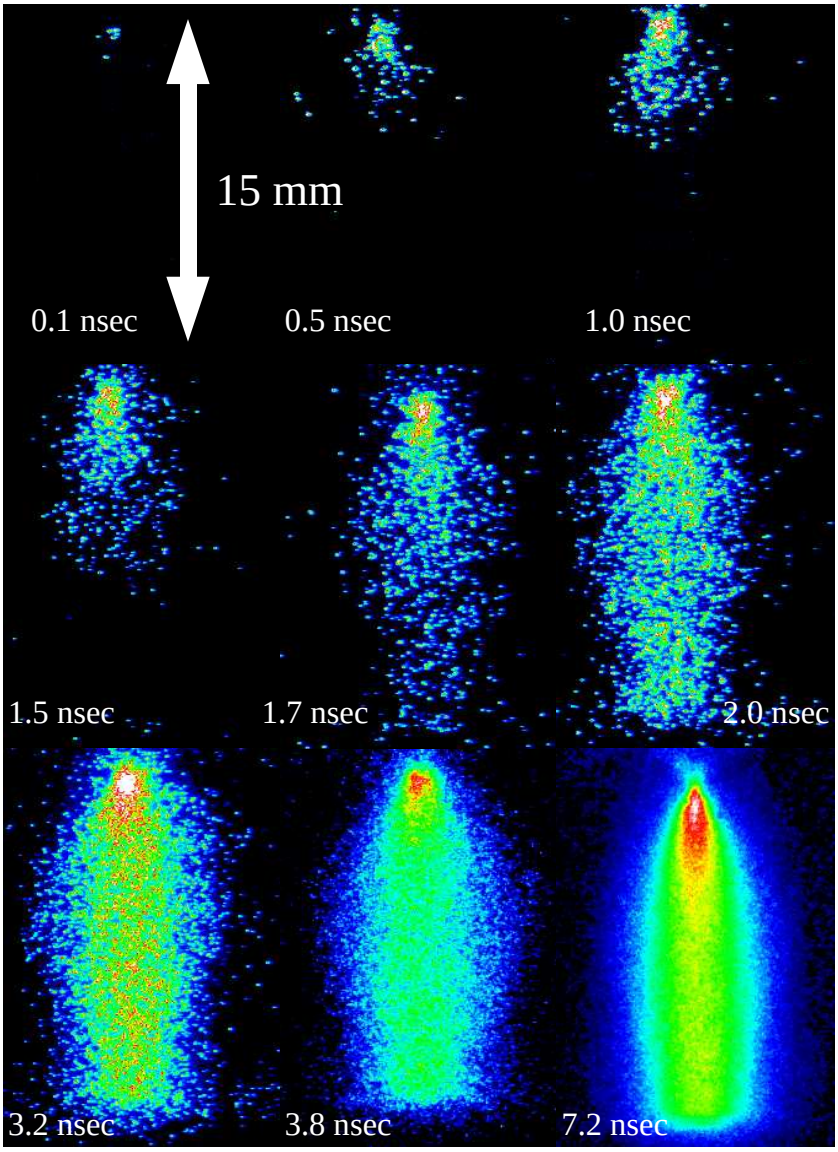

Figure 4.1: Images of negative discharges measured at different delay times. The applied voltage was -40 kV, the pressure was 200 Torr. The grey scale indicates the intensity. For display purpose the scale of each image is different.

4.2, similar pictures are shown for a positive discharge. Positive and negative discharges have a very similar appearance and time evolution. The discharge starts at the point electrode with an avalanche, gradually extends towards the plate electrode (the ionization front) and when the tip of the discharge approaches the plate a single channel develops (breakdown), which increases in light intensity.
It is clear that in the initial stage, the discharge cannot be described by a single channel of emitting ions. Instead the discharge starts simultaneously in several points, scattered over an area of several mm. The density of these points is the highest near the point electrode where the applied electric field is highest. Experimentally, the clear distinction between the three different regions, cathode/anode fall, channel/plateau and ionization front (fig. 2.3) is found to be not very well defined.
Both positive and negative voltage data show that the propagation of the discharge is very rapid. By inspection one can see that at 200 Torr, a negative discharge closes the gap within 2 nsec (fig. 4.1), and a positive discharge in approximately 1.5 nsec (fig. 4.2). Due to this rapid propagation the ionization front can only be studied at very short times, when it is still far away from the plate electrode. The propagation velocity itself is studied in chapter 5.

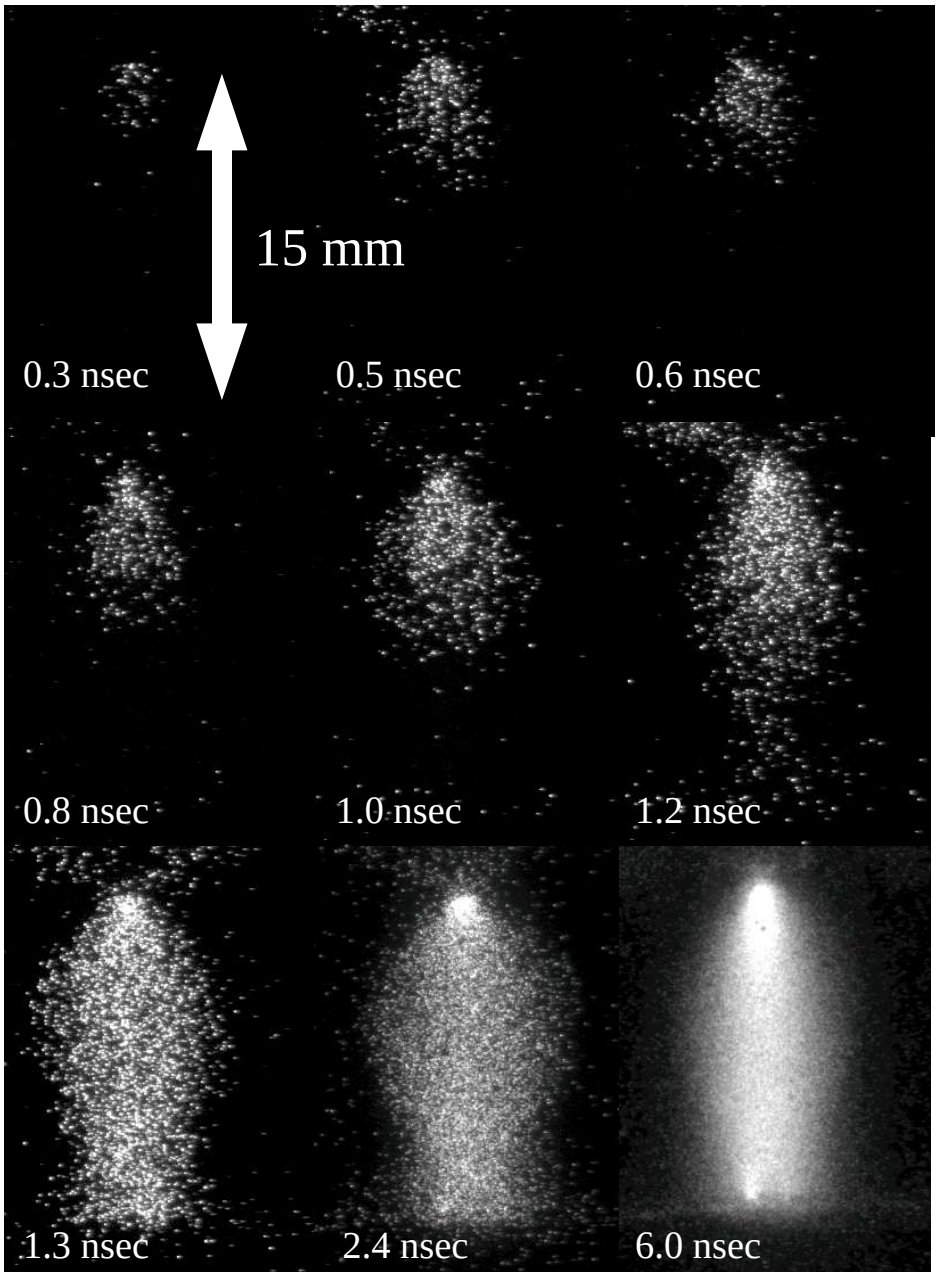

Figure 4.2: As in figure 4.1 but with a positive voltage of 40kV

4.2.2 The ionization front

The most interesting part of the discharge is the evolution of the ionization front which can be studied in the first nsec before the tip reaches the counter-electrode. Recent theoretical work [1,2,3] has concentrated on the slope and the propagation of the ionization front. Specifically it has been predicted that this front should be quite narrow (a few μm wide) and propagates more or less with the same shape (constant wide) through space, converting the neutral atoms ahead into an ionized plasma.
In fig. 4.3 the front for a negative voltage (-40 kV) and in fig 4.4 for a positive voltage (40 kV) is shown in more detail at short time delays.

Roughly speaking the following differences between the front evolution of positive and negative discharges can be seen. At the same (higher) pressure of 600 Torr positive streamers show almost no branching while negative streamers do. Branching is discussed in more detail in section 4.3. The most important information from these data is that in all cases the light intensity at the tip is very spiked and non-uniform, and does not resemble the idealized picture for streamer formation as sketched in fig. 2.3 where the cathode/anode fall, the channel/plateau region and the ionization front can clearly be distinguished. These spikes are orders of magnitude above the noise level of the detection system (they correspond to at least 40 photons) and reflect therefore real pointlike sources of emission of radiation.
This same conclusion also emerges from a study of the width of the active head shown in fig. 4.5, as a cross section of the emitted light intensity at different pressures. This figure confirms the spiked nature of the head but also shows that globally the head is about as wide as it is long. Once again the observed behavior is hard to reconcile with the theoretical predictions in fig. 2.5, which show a propagating finger with fixed width.

To illustrate this spiked nature of the discharge we show in figures 4.6 and 4.7 the behavior of the emitted light as a function of position along the path of the discharge, both as the intensity along a single line of pixels in the center of the discharge path (left panel), and as an average over 10 neighboring lines of pixels (right panel) for both positive and negative discharges and several delay times. All curves show a spiky profile, the onset of which progresses with time. The right panels are obviously more regular with less pronounced spikes, because the intensity is averaged over

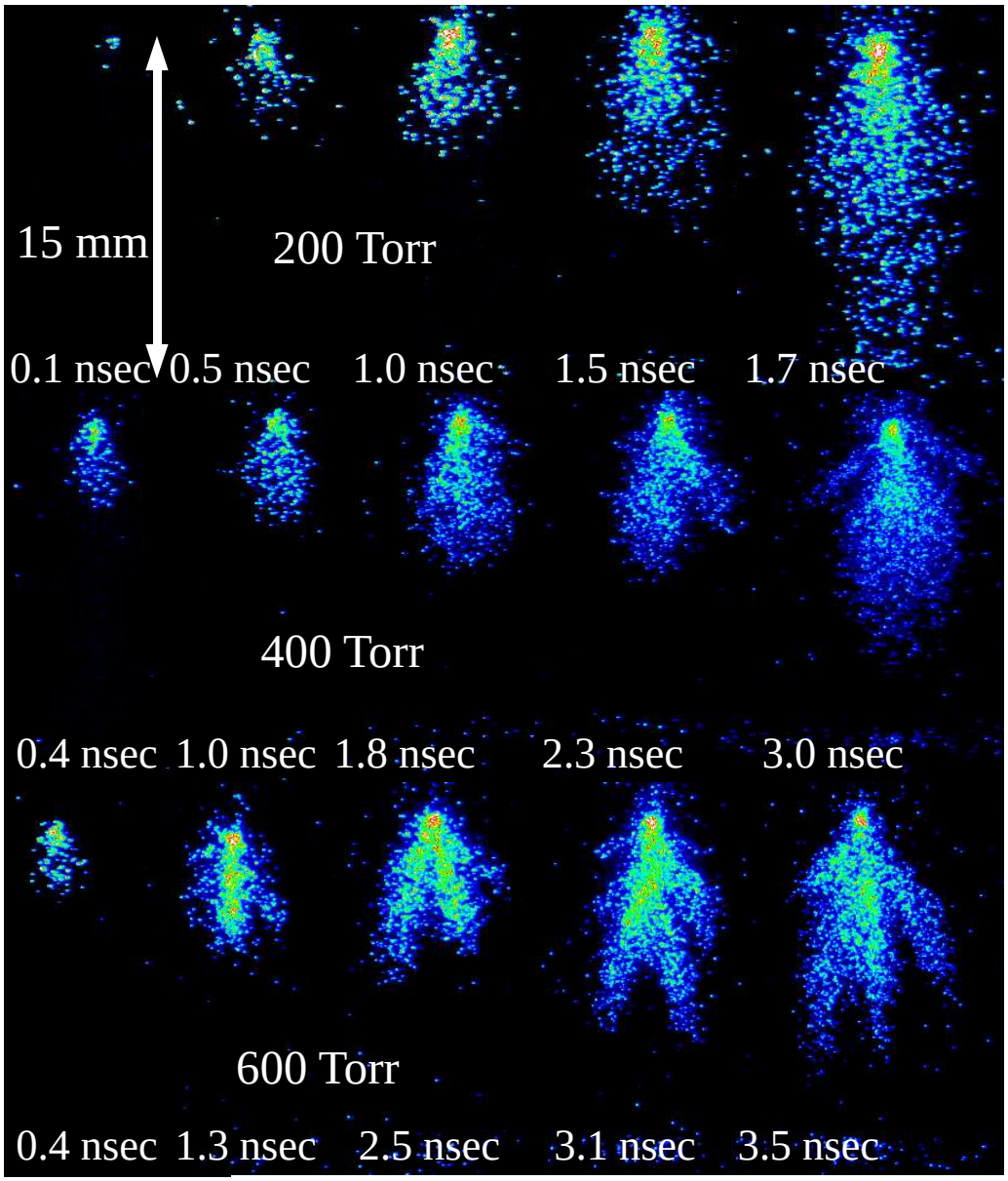

Figure 4.3: The front of the streamer for a negative voltage (-40 kV) as a function of pressure, measured at different delay times.

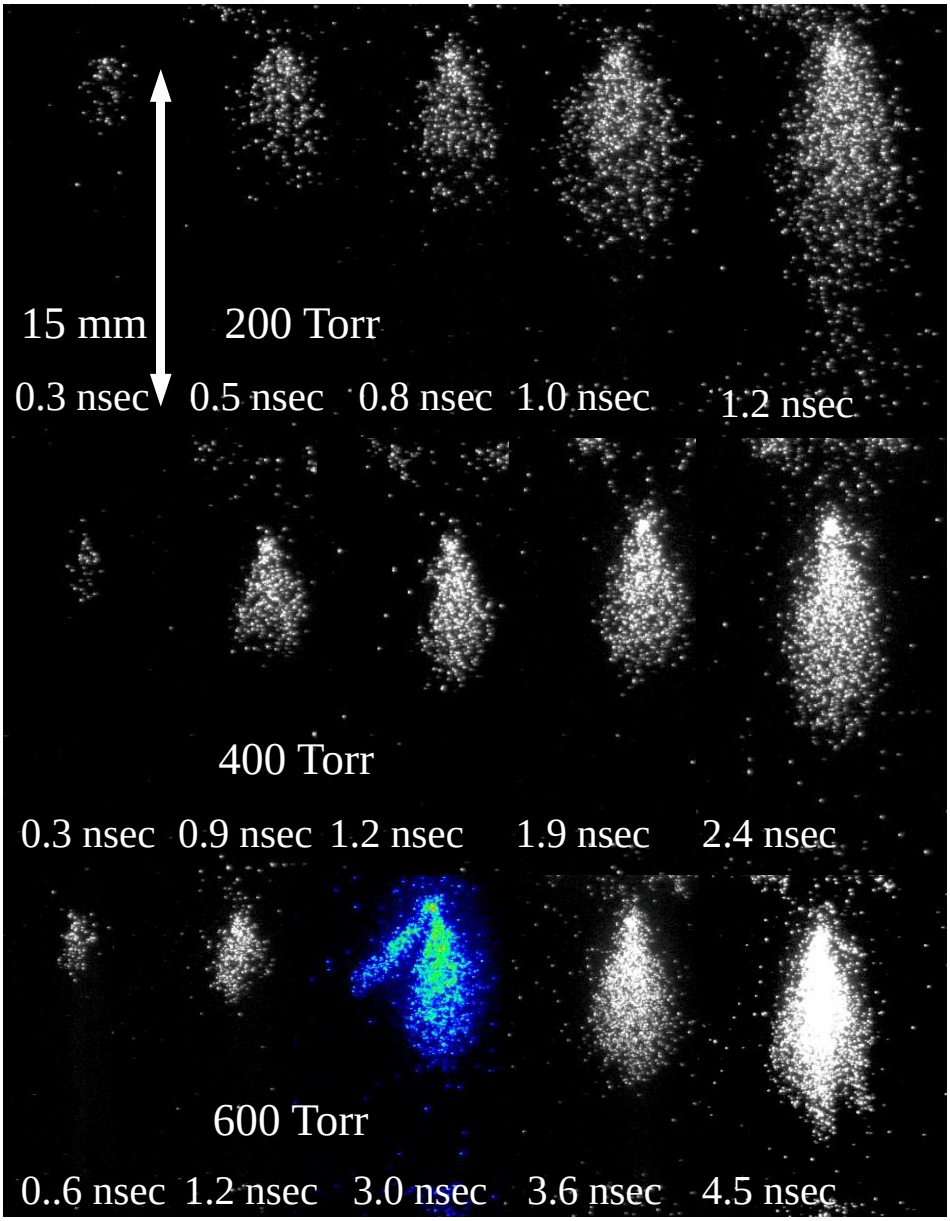

Figure 4.4: The front of the streamer for a positive voltage (40 kV) as a function of pressure, measured at different delay times.

10 lines. It is clear that the averaging procedure leads to a more gradual shape of the intensity profile. By observing the general trend in the averaged curves (right panels) it is possible to detect a general shape of the discharge profile which consists of a region of higher intensity near the electrode and a gradually down sloping intensity, which advances further away from the electrode as time progresses. In all curves we observe that the intensity is high at the point electrode, where there are more and bigger electron avalanches/streamers. This observation is particularly clear in the negative discharge where there is a narrow region of high intensity which is not shifting with time and is therefore clearly associated with

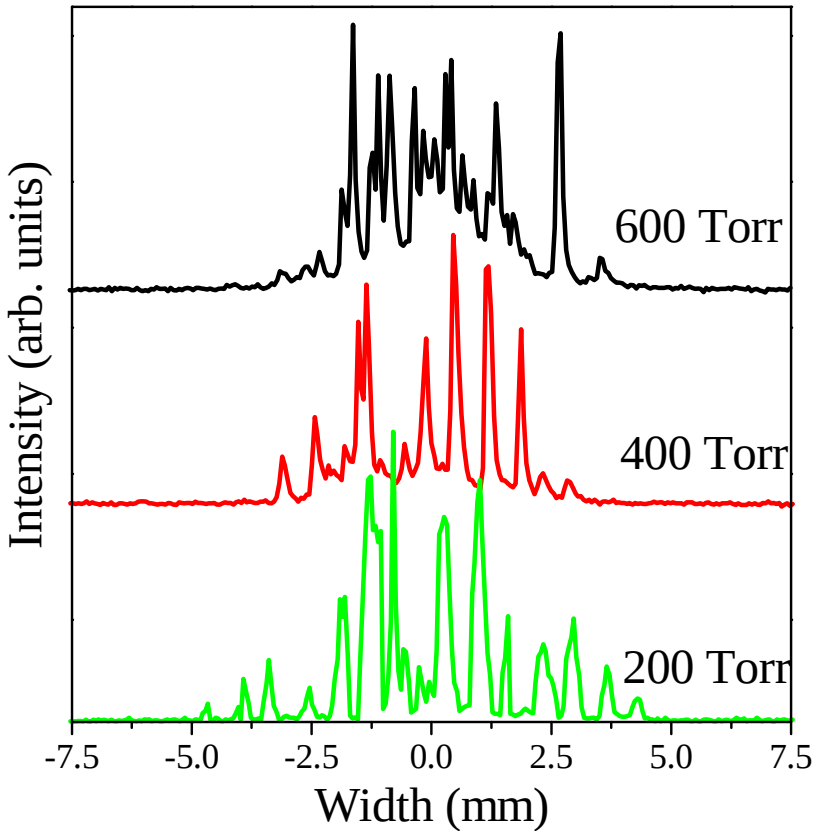

Figure 4.5: The width of the active discharge head for different pressures taken half way the active head for a positive discharge.

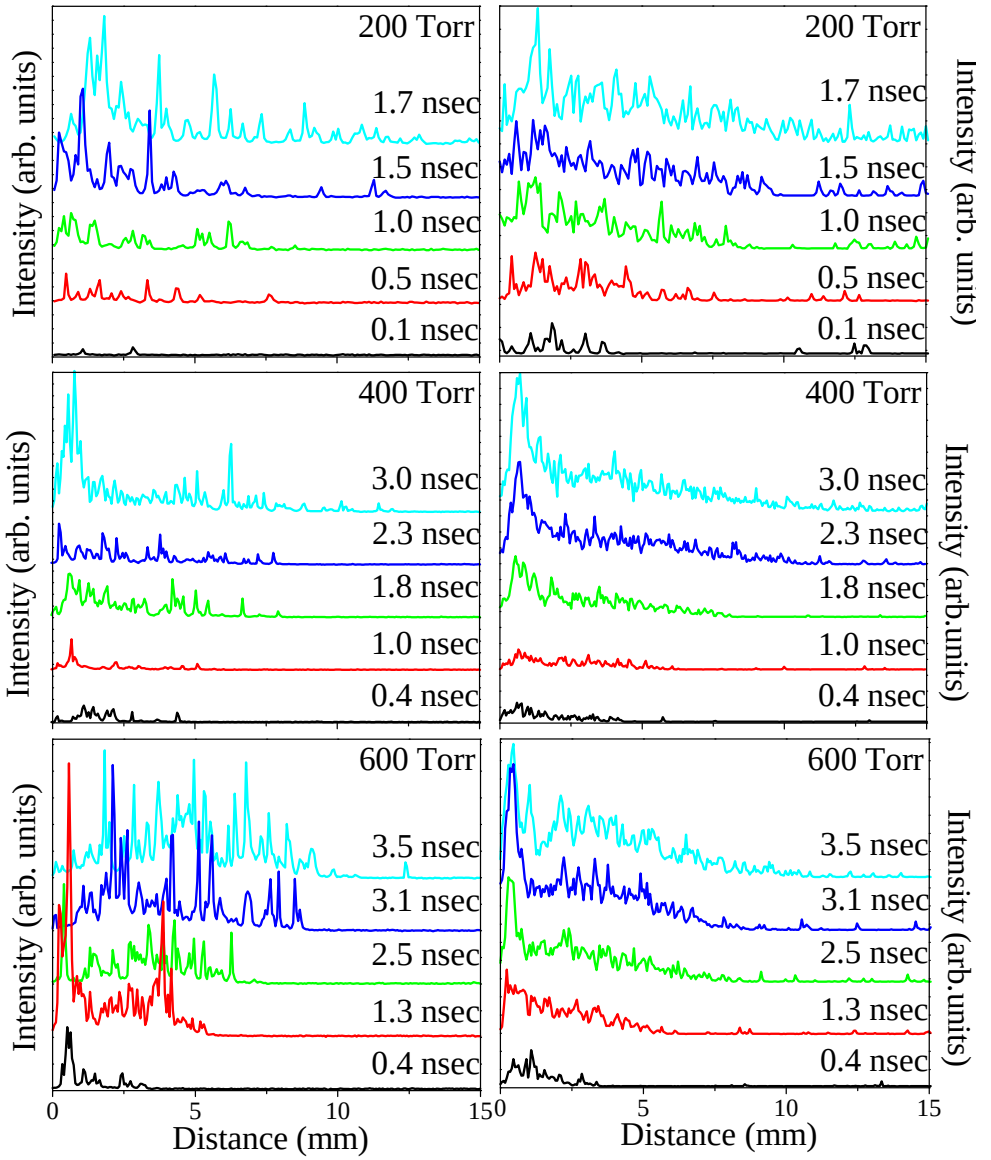

Figure 4.6: The intensity of the streamer as a function of distance (from the tip electrode) and delay for different pressures for a negative discharge (-40 kV). Left panel corresponds to the intensity across a single line, the right is an average over 10 lines.

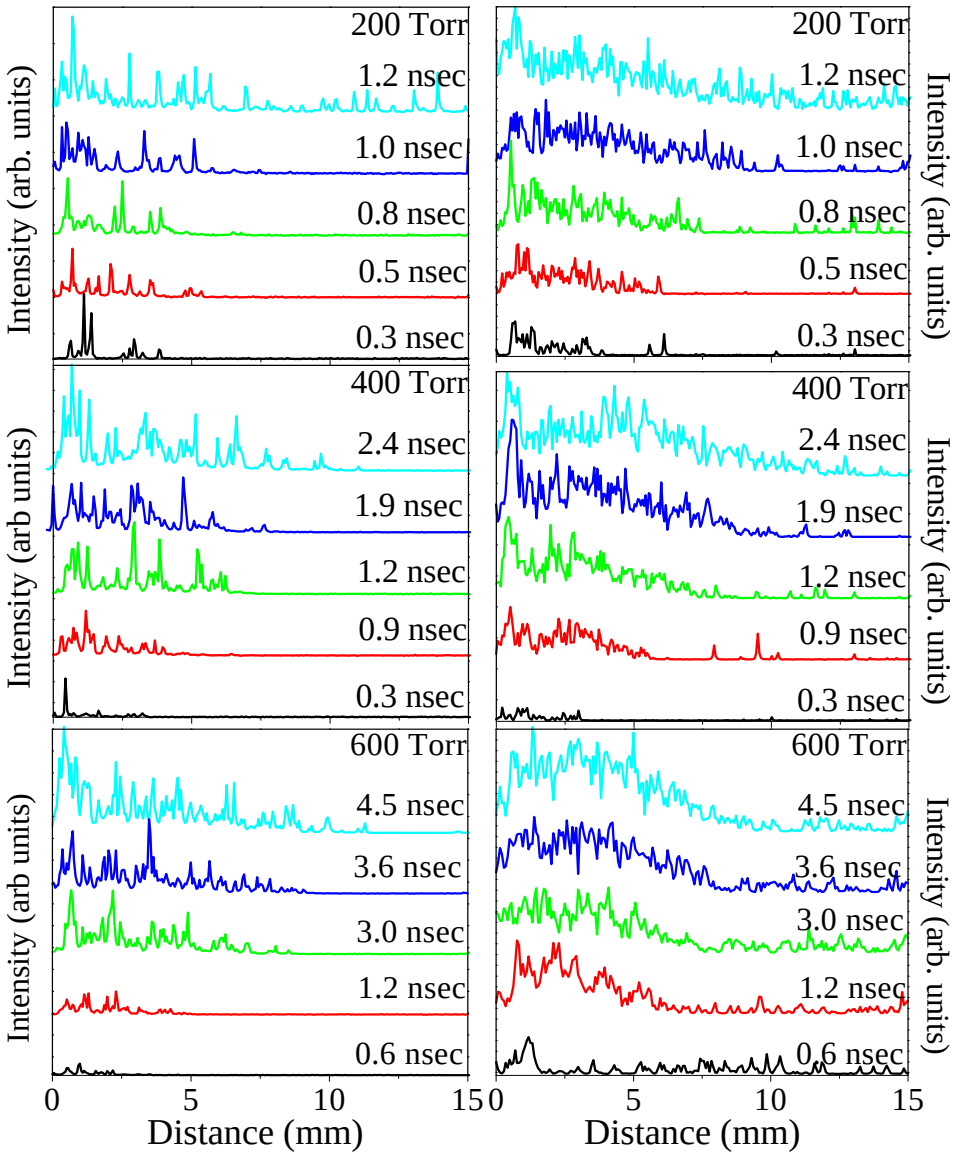

Figure 4.7: The intensity of the streamer as a function of distance (from the tip electrode) and delay for different pressure for a positive discharge (40 kV). Left panel: intensity at a single line. Right panel: average intensity over 10 lines.

the electrode. This initial peak reflects the strong ionization in the cathode/anode fall region. It is seen more clearly in the negative discharge, for which the cathode fall is in generally higher.
The observations can thus be summarized as follows. The spatially averaged intensity indeed show a shape which somewhat resembles the idealized shape in fig. 2.3, with a electrode fall, a channel and a front, although the channel and the front are hard to distinguish. Furthermore in this interpretation the front is very wide (order mm) and not at all the steep front theoretically predicted. However, this averaged intensity profile in fact consists of a sum of very localized points of very high intensity, separated by larger area which are basically dark. We believe therefore that the ionization process starts at many places at the same time, dictated by the presence of free electrons in the neutral gas with sufficient mean free path to ionize. With time and with increasing electric field the density of these avalanches (each light point corresponding to an avalanche) increases and eventually they merge to form the channel.

4.2.3 Discussion

In analyzing the data it is important to bear in mind that the images reflect the time integrated intensity of the discharge from the opening of the shutter of the camera and the start of the discharge. The shutter remains open during five nsec and therefore is open during the whole time in the images we are studying here. Since also the lifetime of the excited atom and molecules is of the order of $\sim$ 1 nsec the images do not reflect the degree of ionization actually present at a certain position and a certain moment. Therefore even if the ionization front would be very sharp and homogeneous, as theoretically predicted, this time integrating effect would tend to smear out all sharp features. More specifically a sharp wavefront with a propagation velocity of 10^6 m/s would show up in the images as a gradually increasing intensity at the front over a length of a mm, as indeed observed in the space averaged pictures. In order to really observe a snapshot of the propagating discharge a camera with a much shorter opening time would be needed and /or the used gas molecules should have a much shorter lifetime, which at present is not realizable. Therefore, the limitations of the experiment pose some constraints on definite statements. However, these limitations do not invalidate the main conclusion from our

data, since timing effects cannot be responsible for the type of speckled images which we always observe. Even though the measured intensities are much higher than the detection threshold of the ICCD camera, the images always show the speckled nature as observed in fig. 4.3 and fig. 4.4, corresponding to the irregular intensity profiles in fig. 4.6 and 4.7. These speckles are therefore not related to noise but really reflect the very inhomogeneous light distribution in the discharge.
We therefore believe that the ionization process in fact starts at very many places at the same time, dictated by the presence of free electrons in the neutral gas with sufficient mean free path to ionize. As the electric field increases the density of these avalanches increases and they eventually form the channel. This channel is not uniformly ionized, but exists of individual avalanches with a concentration that is highest closer to the point electrode.
Another argument which pleads against the temporal smearing of the image as the main cause for the width of the ionization front is found in the figures 4.3 and 4.4. These figures show that with time the cross section of the front becomes wider. I.e. the discharge head grows in the direction perpendicular to the propagation direction. This observation contradicts the theory in which they asuume that the streamer propagates with a constant width, finger like. The width we observe is about equal to the length of the ionization front, which leads us to believe that this front is indeed so wide.
On the basis of our data we imagine the discharge as a discrete set, gradually merging avalanches as sketched in fig. 2.4.
It is not entirely clear how in this framework the electric potential evolves, since in the initial phase there is no continuous conducting channel. It is obvious that as soon as the process starts the electric field further away from the electrode must increase, since this is the mechanism of propagation. However from our emission data this information is difficult to obtain.
In fig 4.8 we schematically sketch how we believe the discharge grows and the potential behaves. At the beginning, when the potential is applied to the electrode, the potential drops in the (still) dielectric gas, according to the geometry of the applied electric field. Subsequently, free electrons present at certain positions in the gas start, individual electron avalanches (second sketch). When these electron avalanches are large enough they

lead to charge separation between free electrons and ionized molecules which causes a local electric field that triggers new avalanches. These avalanches eventually grow out to small conducting paths. In between

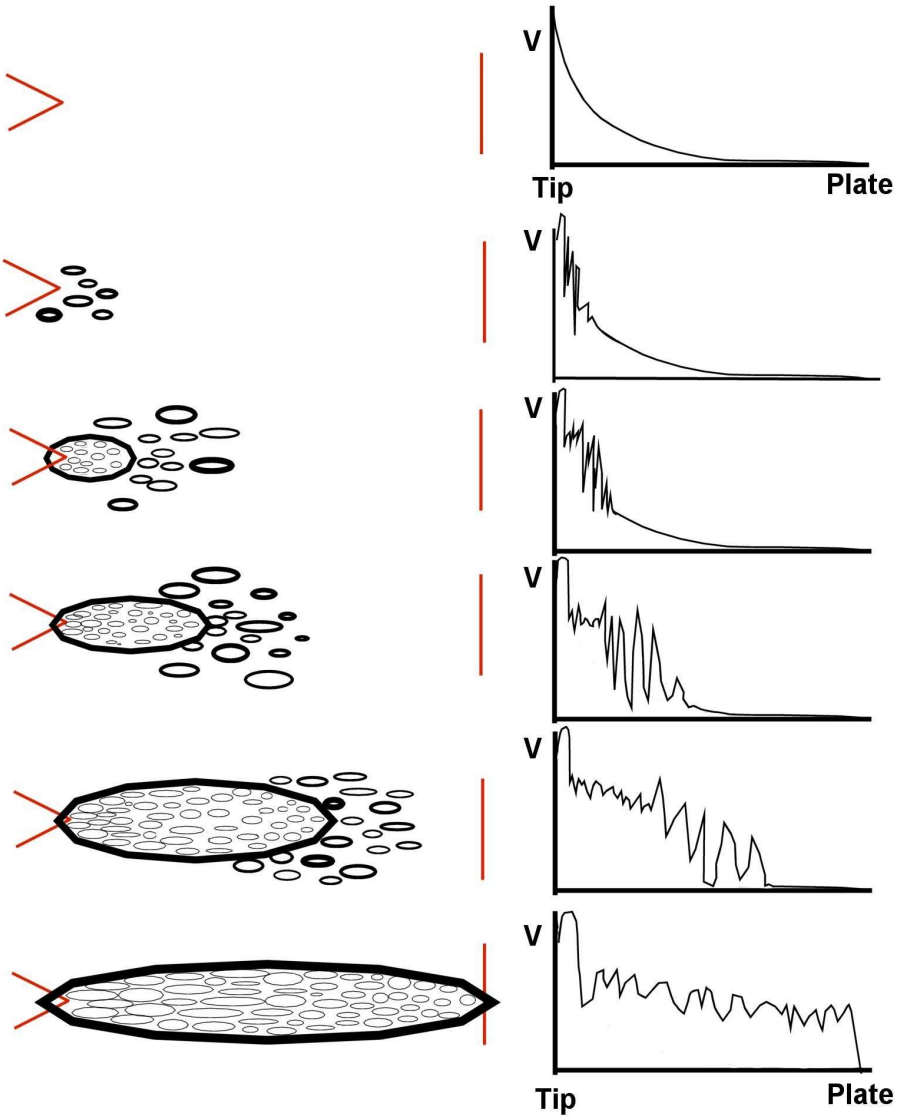

Figure 4.8: Left panel: a schematic drawing of the streamer growth. Right panel: the corresponding behavior of the potential.

these avalanches the gas is still unionized, but may contain already many electrons from earlier avalanches. When the concentration of the individual avalanches is sufficiently high, the (dark) free electrons transfer the potential to the front of the streamer (fourth sketch). In front of the streamer new electron avalanches start to grow making the streamer travelling further towards the other electrode. Our model is therefore a combination of the discrete avalanches in fig. 2.4, combined with the voltage distribution of fig. 2.3, but in a much more irregular fashion, reflecting the random and inhomogeneous nature of the avalanches. The main difference with earlier theoretical descriptions is that we believe that breakdown in fact starts in many places in front of the tip and that the density of avalanches increases both with time and as a function of the distance to the tip. The increasing density of discrete avalanches causes them to merge in what can be called a streamer. We believe that the discrepancy with theoretical models which predict a sharp nature of the ionization front comes from the neglect of the effect of ionization and avalanches initiated by the randomly distributed free electrons initially present in the gas. A crucial element in our mechanism is that in some way the potential at the electrode must be transferred to the tip, in order to create a propagating discharge. In the next sections and chapters we will show that the velocity and the magnetic field measurements provide clear evidence that the potential profile changes and that some of the electrode potential is indeed transferred to the propagating tip.

4.3 Branching of streamers

As can be seen in fig. 4.9 sometimes a streamer splits up in more paths, especially at higher pressures and lower electric fields. The phenomenon which is called branching has been rarely discussed in literature. In general simulations do not reproduce branching [1,2], or only [4] at much higher electric fields. The occurrence of branching implies that the discharge path does not follow anymore the path of the strongest applied electric field, but is rather determined by charge instabilities near the streamer tip due to fluctuations in the local field.
In fig. 4.9 we report three different types of branching. The image in the left panel shows immediate branching at the point electrode, resulting in

the formation of two streamers. We have observed several events like this, and in most cases one of the two is bridging the gap first, subsequently becomes more intense and eventually develops into the main leader channel. This type of branching is most probably due to high field regions at sharp edges of the point electrode and is not related to any instabilities in the bulk of the gas.
A more interesting type of branching is displayed in the middle panel of fig. 4.9, which shows branching at the head of the streamer [4].
We have not observed this kind of events very often, probably because in our case the gap between point and plate electrodes is small and the streamers do not move very far from each other. This kind of branching mostly occurs for negative streamers although sometimes also for positive streamers, as shown in fig 4.4 for 4.5 nsec delay.
The image in the right panel of fig. 4.9 depicts a third type of branching which most often occurs at high pressures and/or low electric fields. Once the discharge has bridged the gap, small discharges start at the plate electrode. These newly started discharges move towards the point electrode, but often meet half-way another streamer, started at the point electrode to form a small conducting channel. The light intensity of such a channel

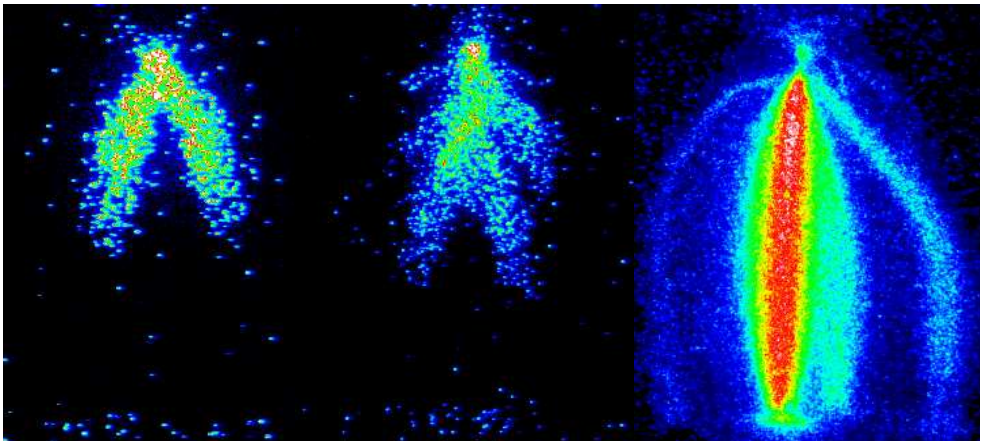

Figure 4.9: Three images of branching discharges, at 600 Torr and -40 kV, electrode branching (left), charge instabilities near the discharge tip (middle), back discharge (right).

always remains low. This branching is therefore a so-called back-discharge, where the degree of ionization of the gas is so high that the weaker electric field at the plate electrode is sufficiently high to start a new branch.
In our numerous experiments we have found that although branching occurs for both negative and positive streamers, their probability is higher for negative streamers. For instance at 600 Torr all negative streamers are branching, sometimes with more than a single bifurcation (middle image fig 4.9).
The frequent occurrence of branching, already at the electric fields used in these investigations is very important, because it supports the idea that the local potential of the propagating streamer at some point is more determined by space charge fields of the discharge itself, rather than by the applied field. Furthermore branching in the middle of a discharge is very easily explained in connection with the results in the previous section, which have shown the importance of random avalanches in front of the tip due to already present free electrons. As soon as the guiding field becomes less important these random events can easily cause bifurcations.

4.4 Electrical results

Historically, many properties of gas discharges have been unravelled by investigating their electrical transients. Measuring the (sub-)nanosecond electrical signals is relatively easy, but the interpretation of the data is often not straightforward, mainly because it is very difficult to obtain any spatial information. With the use of our imaging technique it is now possible to relate the properties of a propagating discharge to the simultaneously measured electrical transients.
The current pulse of a discharge at a particular applied voltage and pressure has been measured by averaging the signal of the current transducer for about 100 discharges. Typical results are shown in fig. 4.10 for different pressures and for a negative (left panel) and a positive (right panel) discharge. The zero time delay taken as the point where the pulse arrives at the discharge chamber, as soon as the current starts to increase and the discharge is starting. The data series in fig. 4.10 reveal some general characteristics which were also found in the imaging experiments discussed in the previous sections.

First, the onset of the current signal occurs later as the pressure increases due to the increasing time which the streamer needs to start (the formation time [5, 6]). The increase in current after the start is steeper for lower pressures, which gives an impression of how quick the total breakdown occurs.
Secondly, the negative discharge and positive discharges exhibit a similar current onset, which implies that the formation time is almost the same for both polarities of the applied field.
In the beginning of the discharge (the first 5 nsec.), as the streamer has not yet closed the gap between the point and plate electrode a very weak current is flowing. This weak current is due to a displacement current, which arises because of the charge separation of the positive and the negative electrons in all the avalanches near the tip. Considering the separated positive and negative charges as a capacitor, we can write:

$$dC = \frac{dQ(x)}{V(x)} \quad \Rightarrow \quad C = \int \frac{dQ}{V} dx \tag{4.1}$$

and the total current is :

$$I = V \frac{dC}{dt} \tag{4.2}$$

$\frac{dC}{dt}$ is the built up of the capacitance as an increasing amount of molecules are ionized and separated from the electrons.

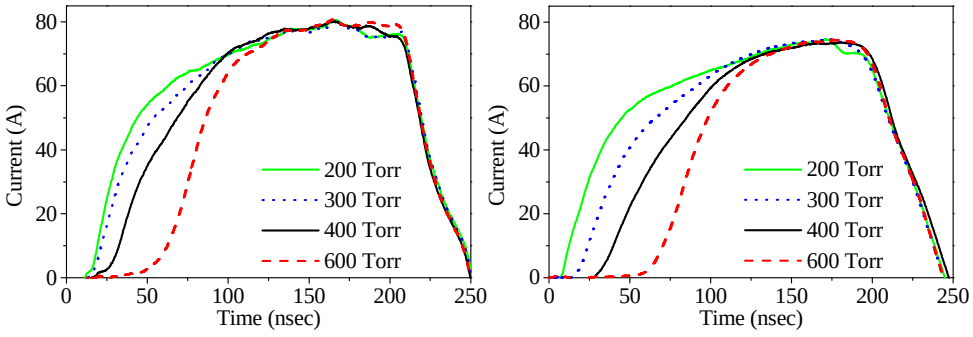

Figure 4.10: Current transients of N_2 discharges measured at 4 different pressures, for a negative discharge -40 kV (left panel) and a positive discharge 40 kV (right panel).

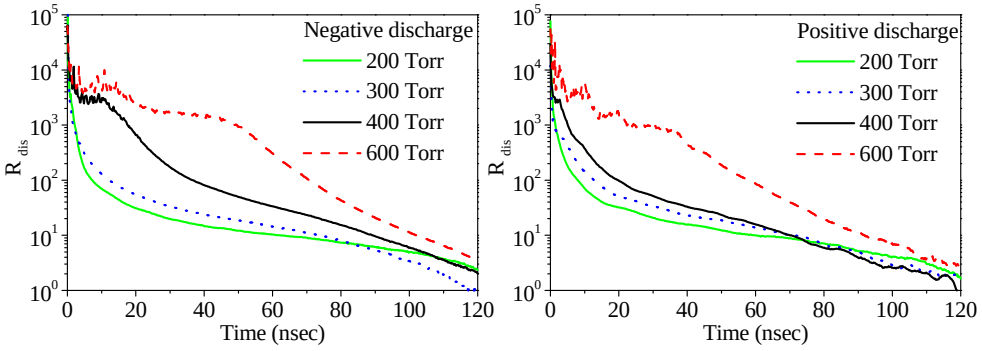

Figure 4.11: The impedance of a discharge as a function of time measured at different pressures, for negative , -40 kv (left panel) and positive discharges, 40 kV (right panel).

Once the gap between the point and plate electrode is closed, a small conducting path, is created and the total current can be written as:

$$I = V\frac{dC}{dt} + \frac{V}{R} \tag{4.3}$$

After a certain amount of time, which depends on the pressure, the channel becomes a good conductor and the current is given by V/R with R the resistance of the fully developed spark.
In order to follow this process, we have determined the impedance of the discharge from the experimental data with use of formula 3.4 (page 42). The results (fig 4.11) show that the impedance around t = 0 and at t>120 nsec. is similar for positive and negative discharges. The different regimes can be clearly distinguished. In the first 5 nsec. a quick decrease of the impedance occurs, due to the charge separation resulting from the ionization of the gas, and the streamer propagates between point and plate electrode. Subsequently, the impedance stays roughly constant for about 8 nsec. when the gap between the electrodes has been bridged by the streamer and the resulting channel is ionized further. The channel heats up and full breakdown occurs, accompanied by a further reduction of the impedance. This scenario is virtually the same for both polarity discharges, with only minor differences in the actual time dependence. In general, all relevant times, that are needed for building up the streamer,

the initial breakdown and the development of a highly conductive fully ionized channel, become longer with increasing pressure. In particular for the negative discharge at 600 torr one can clearly distinguish the 5 nsec. build-up phase, the 15 nsec. of initial breakdown and the full ionization during 30 - 60 nsec.

4.5 Conclusions

4.5.1 The ionization front

All our experiments show a principally different electron density profile as the theoretically expected, figures 2.5 and 2.3. Our data show that the ionization process starts at many places at the same time, dictated by the presence of free electrons in the neutral gas with sufficient mean free path to ionize, leading to a spike-like intensity profile reflecting discrete avalanches. On the other hand it is clear that despite the discrete nature of these avalanches the potential must be transferred to the front of the streamer. We believe that a "conducting"channel is formed which is not uniformly ionized but which, by a combination of (poor) inhomogeneous conductivity and charge build-up, transfers the electrode potential to the tip. The degree of ionization depends on pressure, voltage and time or distance to the electrode. At longer times, higher voltages and nearer to the electrode, the degree of ionization increases and more and more a conducting channel is created. In fig 4.8 we have given a schematic description of how we imagine that this process takes place.

4.5.2 Branching of the streamer

Branching occurs for positive as well as for negative streamers at high pressures or low electric fields, when the random nature of the ionization is more important. Branching in positive streamers is less frequent because the electric field falls more rapidly in front of the head of the streamer than sideways of the streamer. Therefore, the electron avalanches move more easily towards the head of the streamer than to its side.
Negative streamers branch more often, because of the different propagation mechanism. The electrons move out of the tip in all directions and

it is possible that because of collisions they move out of the channel. All these "lost"electrons can start their own streamer. Fig. 4.9 (middle) shows that some streamers branch more than 4 times.
Branching clearly shows that the potential distribution and the local electric field are caused by accumulated charge and the formation of conducting channels in the previous stages of the discharge.

4.5.3 Electrical results

The electrical measurements show basically the same findings for positive as well as for negative discharge. The formation time is the same for both negative and positive discharges. In both cases we can distinguish three phases, a build-up phase where ionization and charge separation takes place, followed by a bridging of the gap with a resistive channel, which heats up leading eventually to on almost vanishing resistance in the final breakdown.

4.6 Bibliography

[1] P.A. Vitello, B.M. Penetrante, and J.N. Bardsley, Phys. Rev. E **49**, 5574 (1994)

[2] S.K. Dhali, and P.F. Williams, Phys Rev. A **31**, 1219 (1985): J. Appl. Phys **62**, 4696 (1987).

[3] Ute Ebert, Wim van Saarloos, and Christiane Caroli, Phys. Rev. Lett. **77**, 4178 (1996), Phys. Rev. E **55**, 1530 (1997).

[4] Manuel Arrayás, Ute Ebert, and Willem Hundsdorfer, Phys. Rev. Lett. **88** (2002), 174502.

[5] Yu. R. Raizer, *Gas discharge physics*, Springer-Verlag, Berlin, New York 1991.

[6] G.F. Westron, *Cold cathode glow discharge tubes*, ILIFFE books london 1968.

Chapter 5

Propagation velocity of negative and positive streamers

Introduction

The propagation velocity of negative and positive streamers in air or nitrogen has been intensively studied, but the reported values differ by an order of magnitude [1-10]. Partially this difference can be attributed to the measurement techniques and electrode geometries used. It is generally assumed that the propagation velocity scales with E/p, with E the electric field and p the inverse pressure. The reason behind this scaling is that the electron energy after acceleration in a field E is $e \cdot E \cdot l$ for a mean free path of l. l depends on the average distance between molecules which is proportional to the inverse pressure. Therefore for the same E/p the average electron energy and thus the rate of ionization is the same.
By historical convention E is expressed in V/cm and the pressure in Torr. Our experiments cover the range $E/p = 40$ till $E/p = 140$ V cm^{-1} torr^{-1}. Most experiments have been carried out in overvolted gaps, with both cathode-directed (positive) and anode-directed (negative) streamers. The discharge is triggered by some external means, such as laser excitation, in

the middle of the gap between the electrodes, mostly in a plate-plate geometry. Both cathode and anode-directed streamers start simultaneously. Other experiments have been performed in the same manner as ours, using a point electrode at which only one streamer is starting. This configuration has the advantage that streamers of both polarities can be studied separately. A disadvantage is the uncertainty of the exact time when the discharge starts, but we have overcome this problem, as explained in chapter 3.

With overvolted gaps Wagner [1, 2] studied the velocity of streamers with E/p of 55 V cm^{-1} torr^{-1} . He reported that anode-directed streamers have a speed of $4 \cdot 10^5$ m/s and cathode-directed streamers a speed of, $1 \cdot 10^5$ m/s. Chalmers *et al* [3] have varied the E/p values from 45 to 55 V cm^{-1} torr^{-1}. The velocity of the anode-directed streamer changed from 1 to $6{\cdot}10^5$ m/s. Strizke *et al* [4] found the speed to be $5{\cdot}10^5$ m/s for anode-directed, and $1{\cdot}10^5$ m/s for cathode-directed streamers for E/p 50 V cm^{-1} torr^{-1}. All cathode-directed streamers show almost the same velocity, but the measured velocities of anode directed streamers change very substantially.

In experiments with point-plate geometry, Dougal and Williams [5] reported a velocity of $2{\cdot}10^6$ m/s for a cathode-directed streamer with E/p 42 V cm^{-1} torr^{-1}. The conditions in this report are similar to ours, except that the streamer was initiated by a YAG laser, which also interacts with the propagating streamer. Peterkin and Williams [6] reported observations of streamers in a trigatron spark gap. They found propagation velocities of 1.7 to 3.6 $\cdot 10^6$ m/s for E/p ranging from 26 to 34 V cm^{-1} torr^{-1}, for both cathode and anode directed streamers. The most extensive study so far has been done by Won and Williams [7], who studied anode and cathode directed streamers in nitrogen with a gap between the point and plate electrode of 13 cm. They have varied the E/p values from 10 to 90 V cm^{-1} torr^{-1}. Thereby the speed of the cathode directed streamer varied from 0.3 to 11 $\cdot 10^6$ m/s and of anode directed streamers from 1 to 7 $\cdot 10^6$ m/s.

The propagation velocity for overvolted gaps are approximately one order of magnitude smaller then the values found by the second group of experiments. Most of these experiments are hard to compare because of the sometimes very different experimental conditions. Despite these uncertainties in the propagation velocity a few conclusions have emerged

from these experiments so far. For instance, the minimum propagation velocity necessary for a streamer to develop [8], is found to be $1 \cdot 10^5$ m/s in air and $5 \cdot 10^4$ m/s [9] in nitrogen. The lower minimum velocity in nitrogen is generally attributed to a lower density of negative ions in nitrogen than in air.
A further complication in determining and comparing streamer velocity is due to the dependence on the length of the discharge [10]. Observations of a cathode directed streamer with a length of 40 cm gave the following values for the average velocity along the path length:

length (cm)	0 - 6	6 - 13	13 - 23	23 - 30
speed (m s^{-1})	$4.4 \cdot 10^6$	$3.5 \cdot 10^6$	$1.0 \cdot 10^6$	$6.0 \cdot 10^5$

In this work we will determine the streamer propagation velocity as a function of the electric field (both amplitude and sign) and pressure using the same point-plate configuration (15 mm separation) where a high voltage pulse was applied to the point electrode. We believe that the experimental conditions in our case are better defined and expect that these results are more suitable for theoretical analysis.

5.1 Experimental determination of the streamer velocity

5.1.1 Negative discharges

From images as shown in section 4.2 the distance that the streamer travels in a certain amount of time can be measured. In practice the streamer tip is determined by the position at which the averaged light intensity decreases to 5 % of the maximum. We have defined the propagation length as the distance between the streamer tip and the point electrode. As explained in chapter 3 we can deduce the elapsed time from the electrical data. The final results of negative streamers as a function of pressure are shown in fig. 5.1. We only considered data up to a length of 10 mm because beyond this position often back-discharges occur, i.e. a discharge originating at the plate towards the streamer tip. The figure

shows that for the lowest pressures (200 and 300 Torr) the discharge moves rather quickly with constant speed. For higher pressures (400 and 600 Torr) it seems that the velocity is not constant in time. However we will ignore these deviations from linearity and approximate the data with a constant velocity which overall gives a good description. The solid curves in fig. 5.1 reflect the best linear fit through the data points and fig. 5.2a plots the resulting velocity as a function of pressure. The velocity decreases with increasing pressure, which reflects the shortening of the electron mean free path with increasing density (=pressure). In order to characterize the pressure dependence of the streamer velocity we have

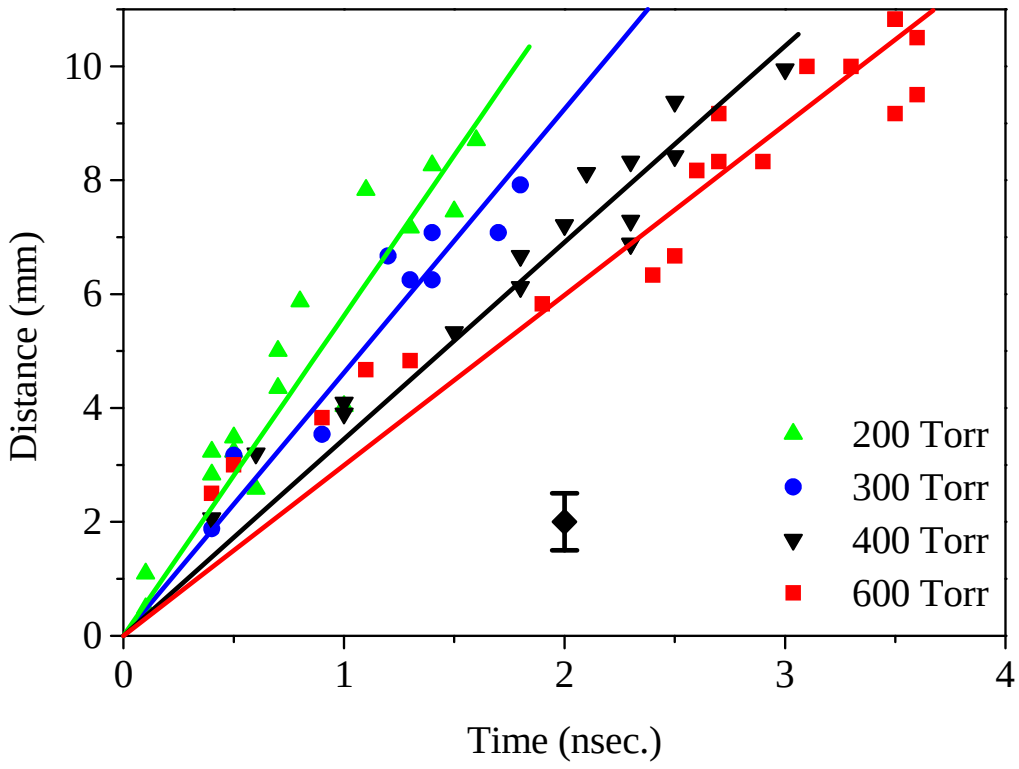

Figure 5.1: The distance the discharge has travelled as function of time, for different pressures and a constant voltage between the point and plate electrodes of -40 kV. The bar indicates a estimated error mainly caused by the fluctuating nature of the discharge front.

fitted the data points to a $v \sim p^a$ power law. The best fit(the grey line) is obtained with a= -0.60 $\pm$ 0.07. For comparison we have also plotted the curve using a *1/p* dependence (a=-1.0 black line) which is expected from Townsend like discharges, but which clearly deviates significantly from the experiment.
Similarly we have studied the voltage dependence at constant pressure by changing the applied voltage between -45 kV to -25 kV (fig. 5.2b). The experiment demonstrates an increasing propagation velocity with an increasing applied voltage, which qualitatively can be explained by the increase of ionizing collisions with increasing voltage i.e. increasing electric fields. The solid curves compare a power law with $v \sim V^{1.58}$ (grey line) and an expected linear dependence $v \sim V$ (black line) with the experimental data. In this case both descriptions reproduce the experimentally determined dependency reasonably well.

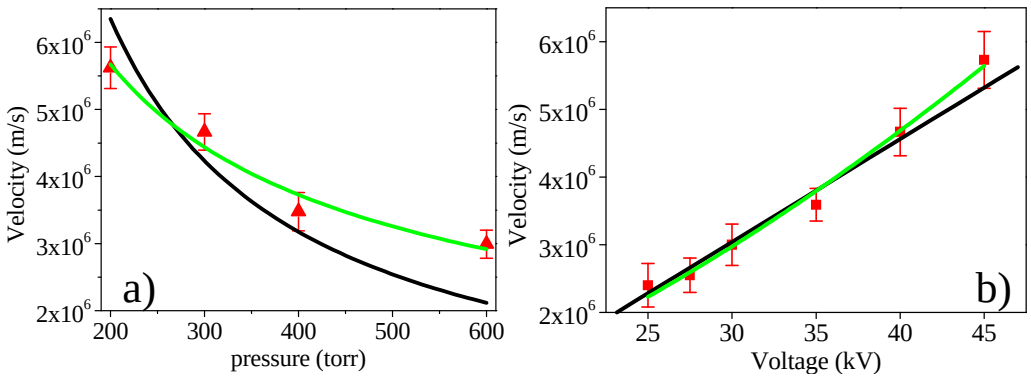

Figure 5.2: a) The streamer velocity as a function of pressure, with constant point-plate voltage (-40 kV). The black line is a 1/p fit and the grey line is the best fit through the measurements using a $p^{-0.6}$ dependence. b) The streamer velocity as a function of voltage, with constant pressure (300 Torr). The black line is a linear fit and the grey line is the best fit through the measurements using a $V^{1.58}$ dependence.

5.1.2 Positive discharges

Similar as for negative streamers we have determined the propagation velocities of positive streamers as a function of pressure at fixed voltage (see fig. 5.3). Also here the data reveal streamers with an extension that grows more or less linearly with time, indicating a constant propagation velocity. As a matter of fact, for positive discharges the velocity is constant for all measured pressures and all delay times, in contrast to negative streamers which exhibited some deviations from linear propagation at higher pressures. The velocity decreases with increasing pressure, and increases with increasing voltage (fig. 5.4a and b). The pressure de-

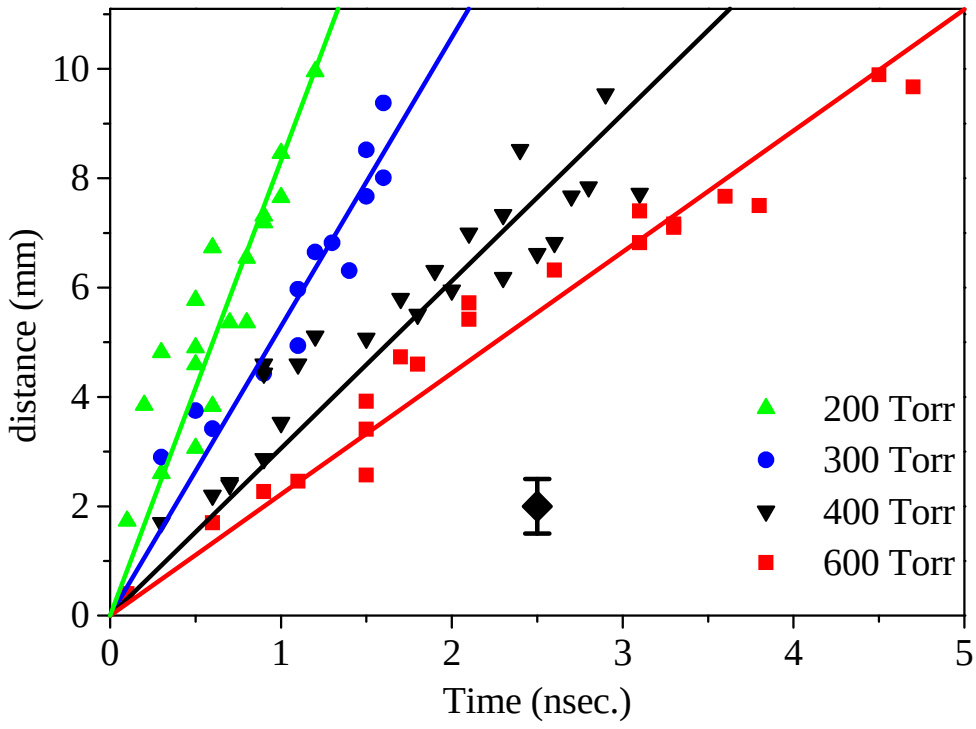

Figure 5.3: The distance the discharge has travelled as a function of time, for different pressures, and a positive applied voltage of 40 kV. The bar indicates a estimated error mainly caused by the fluctuating nature of the discharge front.

pendence of positive streamers is stronger than for negative ones, which is also apparent from the best power law fit through the data (grey line fig. 5.4a) with a = -1.3 instead of a = -0.6 (fig. 5.2a). Also the voltage dependence is stronger than for negative (grey line fig. 5.4b) with a = 2.47 instead of a = 1.58 (fig. 5.2b).

5.2 Discussion

The most striking result from the data is that streamers propagate with a more or less constant velocity. Under our experimental conditions, i.e. in point-plate geometry, the applied electric field profile is essentially non-homogeneous which makes that when the discharge propagates it feels a lower applied electric field. Since at a fixed pressure, the electrical field is the most important parameter to determine the propagation velocity, one expects a reduction of the speed of the ionization front, when the distance from the point electrode increases. Instead the experiments show a constant propagation velocity. The only exception is maybe the deviations from linearity at higher pressures for negative

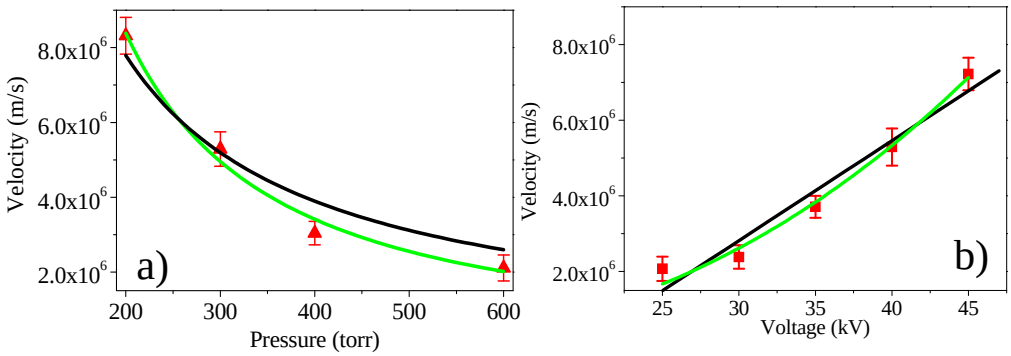

Figure 5.4: a) The streamer velocity as a function of pressure, and constant electric field (40 kV). The black line is a $1/p$ fit and the grey line is the best fit through the measurements, $p^{-1.3}$. b) The streamer velocity as a function of voltage (electric field), with a constant pressure (300 Torr). The black line is a linear fit and the grey line is the best fit through the measurements, $V^{2.47}$.

discharges. We believe that this observation shows that the electric field near the ionization front is more or less the same as at the point electrode. The reason is that the ionized channel despite the irregular nature of the avalanches (chapter 4) transfers most of the electrode potential to the tip of the propagating streamer. This mechanism would explain a more or less constant propagation velocity, despite the inhomogeneous electric field. In this model the velocity is therefore essentially determined by the tip field, which is controlled by the electrode potential. This picture also explains the onset of a back-discharge, starting at the plate electrode when the ionization front comes within a few mm of this electrode. Furthermore, a similar conclusion regarding the importance of the electric field of the streamer tip, can be drawn from our measurements in a magnetic field, which will be described in the next chapter.
Within this framework the difference in propagation velocity of positive and negative streamers directly reveals the different potential near the ionization front. Positive streamers are built from free electrons moving towards the tip, ionizing additional molecules in the process. Therefore the plasma channel in front of the tip (or the electrode at the onset of the streamer) is electrostatically essentially neutral. For negative streamers, electrons are accelerated away from the tip leaving charged ions behind. This space charge would rapidly screen the applied electric field from the electrode and extinguish the streamer. However cold electrons emitted from the electrode (through the cathode fall) will partially neutralize the positive charge left behind by the ionizing electrons. Effectively this will lead to a lower tip field for negative streamers than for positive ones, and thus to a lower propagation velocity, as indeed observed.
One other important issue investigated in the previous section is the pressure and electric field dependence of the streamer velocity. The question is whether it scales with E/p (externally applied) or not. Qualitatively, the propagation velocity of both negative and positive streamers, is higher in increasing electric field and decreasing pressure. This behavior can be understood as a decreasing carrier multiplication by impact ionization as the average kinetic energy of accelerated free electrons decreases as explained in the introduction of this chapter.

Fig. 5.5 summarize the results of fig. 5.2 and 5.4, but scaled in E/p. Obviously the applied electric field is very inhomogeneous due to the point-plate geometry and therefore the horizontal axis in fig. 5.5 is taken

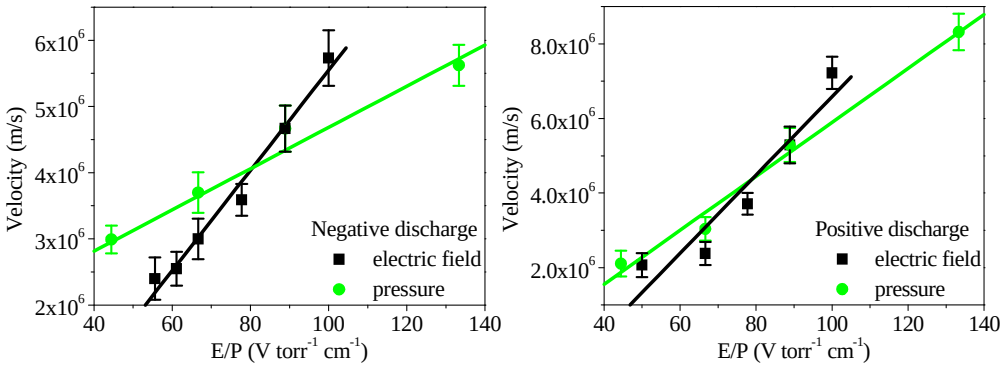

Figure 5.5: The streamer velocity plotted as function of E/p by changing electric field (squares) and by changing pressure (circles), for negative (left) and positive (right) streamers.

as the applied voltage divided by the distance between the electrodes (15 mm). Despite the position dependence of the electric field.
Furthermore since a large part of the applied voltage is transferred to the streamer tip during propagation, the voltage just behind the streamer tip is constant and the decrease of the voltage in front of the tip depends merely on the properties of the gas.
It follows from fig. 5.5 that in general E/p scaling of the streamer velocity is not valid. For positive streamers the E/p scaling can work reasonably well, at least within the experimental error, whereas for negative streamers we have observed clear deviations. In particular the electric field dependence seems more strong than the pressure dependence. Our observations therefore confirm the results of previous reports [7] regarding the absence of E/p scaling, which partially explains the wide variety of reported streamer propagation velocities.
We believe that the high precision of our measurements leads to a reliable determination of the streamer velocities at different experimental conditions. We hope our experiments stimulate further theoretical work to calculate the proper propagation velocities.

5.3 Bibliography

[1] K.H. Wagner, Z. Phys. **189**, (1966), 465

[2] K.H. Wagner, Z. Phys. **204**, (1967), 177

[3] L.D. Chalmers, H. Duffy, and D.J. Tedford, Proc. R. Soc. Lond. A **329**, (1972), 171

[4] P. Stritzke, I. Sander, and H. Raether, J. Phys. D **10**, (1977), 2285

[5] R.A. Dougal, and P.F. Williams, J. Phys. D: Appl. Phys. **17** (1984), 903

[6] F.E. Peterkin, and P.F. Williams, Appl. Phys. Lett. **53** (1988), 182

[7] J.Yi Won, and P.F. Williams, J. Phys. D: Appl. Phys. **35** (2002), 205

[8] E.M. Bazelyan, and A. Yu Gorjunov, Elektrichestov, **11**, (1986), 27

[9] E.M. Bazelyan, and A. Yu Gorjunov, Izu. Akad. Nauk. SSSR, Energetika transp., **4**, (1982), 75

[10] Positive discharges in Air Gaps at Les Renardieres - 1975 results. By the 'Les Renardiers Group', Electra **53**, (1977), 31

Chapter 6

Discharges in magnetic field

Introduction

Two important issues concerning the properties of electrical gas discharges in ionizing electric fields, which are not answered until now, are the possible role of photoionization in the discharge process and at which point the applied guiding field responsible for the beginning of the discharge is overcome by the electric field caused by the space charge created in the ionization process. In this chapter we will describe how a study of discharges in a magnetic field can be used to study these issues.

A magnetic field gives rise to an additional Lorentz force on a particles with charge q, mass m that moves with velocity $\mathbf{v}$ in an electric field $\mathbf{E}$:

$$\mathbf{F} = q(\mathbf{E} + \mathbf{v} \times \mathbf{B}) \tag{6.1}$$

The motion of charged particles is characterized by a few terms:

■ A circular movement around $\mathbf{B}$ with a cyclotron frequency of $\omega_c = qB/m$

■ An accelerated motion of this circular motion along $\mathbf{B}$ with $\dot{v}_s = qE_{\|}/m$, with $\mathrm{E}_{\|}$ being the component of $\mathbf{E}$ parallel to $\mathbf{B}$

■ A constant drift of the guiding center perpendicular to **B** and **E** with the drift velocity $v_\perp = E_\perp/\mathbf{B}$, with $E_\perp$ being the component of **E** perpendicular to **B**

The circular cyclotron motion is much too rapid and the orbit much too small to be observable and we are therefore only interested in the drift motion, which for a particle with a collision time τ is given by:

$$m\dot{v} \;=\; -e\mathbf{E} \;-\; e\mathbf{v} \;\times\; \mathbf{B} \;-\; \frac{m\mathbf{v}}{\tau} \tag{6.2}$$

This equation is the well known drift equation for particles in crossed electric and magnetic fields. In a homogeneous electric field it can easily be shown that the drift motion occurs in a direction which makes an angle Θ_H with the applied electric field. Θ_H is determined by [1]:

$$\mathrm{tan}\Theta_\mathrm{H} \;=\; \frac{\mathrm{eB}}{\mathrm{m}}\tau. \tag{6.3}$$

This so-called Hall angle does not depend on the sign nor on the amplitude of the electric field. Therefore, for a pure radial electric field (the so-called Corbino geometry) the motion can directly be seen to be a logarithmic spiral where the particle always makes the same Hall angle with respect to the local, radially directed electric field. In the present case the electric field is an inhomogeneous dipole field for which no simple analytic expressions for the motion can be given. However also in this case the trajectories can easily be constructed by imposing that at any position the drift motion will be at an angle Θ_H with the electric field.
In fig. 6.1 we show the drift motion in this geometry. Since the Hall angle does not depend on the sign and the magnitude of the electric field, the path for a particle with a specific charge is the same for positive as for negative voltage. Therefore the curvature of the path remains the same even when the direction of the electric field is inverted.
It is reasonable to assume that the path of a discharge will follow the average motion of drifting particles. We therefore expect that the discharge

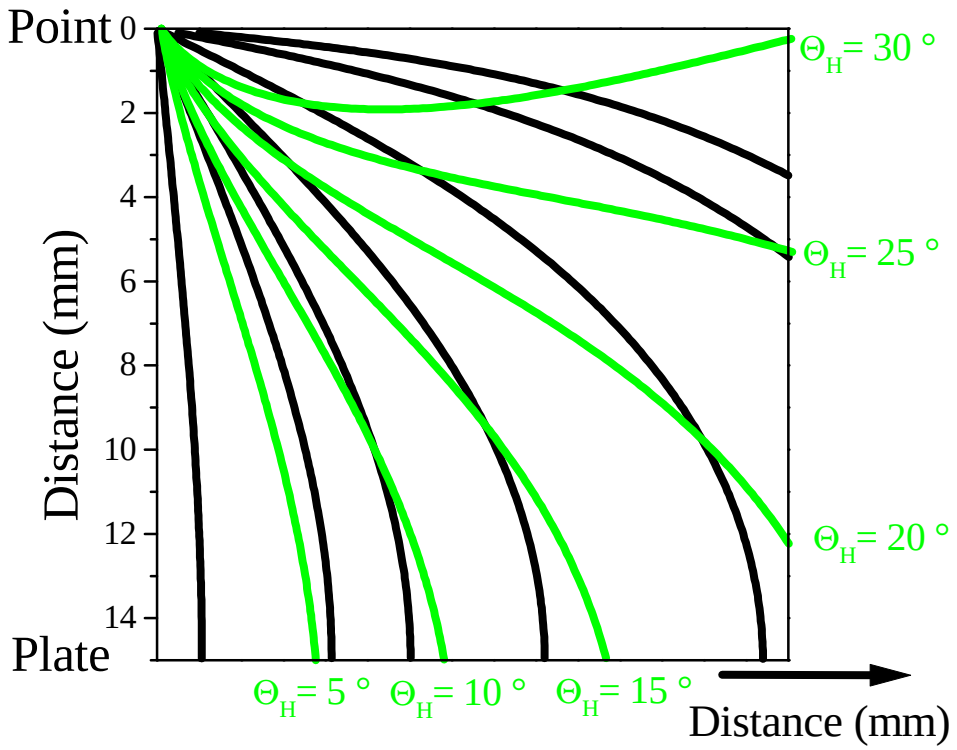

Figure 6.1: The path the streamer (the grey lines) will follow with a constant Θ_H. The black lines are the electric field lines.

in a magnetic field will show a path which will start at the tip and which propagates at a constant angle with the direction of the strongest electric field. In the initial phase this field will be directed straight forward towards the plate electrode. As the discharge propagates the path will become deflected sideways and will change direction continuously.
If photoionization is the most important carrier multiplication mechanism a different behavior will occur. Photons are not affected by the magnetic field and therefore the deionizations by photons will statistically occur at the same positions as without magnetic field somewhere in front of the tip. Consequently no deviations from the zero magnetic field path are expected for photoionization.

When the electric field starts to deviate substantially from the applied guiding field also deviations from the calculated path are expected because the electric field direction will be different. Such deviations will not occur in the initial phase, when space charge effects are still unimportant but will show up when the ionization front has proceeded some distance from the tip.

6.1 Influence of the magnetic field on the discharge

In the measurements presented in this chapter the direction of the magnetic field is always perpendicular to that of the electric field and the growth direction of the discharge. In fig. 6.2 the magnetic field direction is perpendicular to the plane of the paper, out of the paper. The measurements have been done at a constant pressure (200 Torr) and constant voltage (-40 kV). The figure shows the propagation of the discharge for different magnetic fields, at 5 Tesla (top panel), 10 Tesla (middle) and 12.5 Tesla (bottom). A clear deviation from straight propagation is visible, exhibiting an anti-clockwise curvature. Fig. 6.3 shows the discharge in a oppositely directed magnetic field of 7.5 Tesla, into the paper. Here the pressure was 400 Torr and the voltage -40kV. As expected the reversal of the field leads to an opposite direction of the curvature.
As discussed above (eq. 6.3) the Hall angle does not depend on the absolute value nor on the direction of the electric field. To verify this fact we have measured the path of the discharge for a positive voltage (see fig. 6.4). The measurements have been done at 400 Torr at a voltage of 40 kV for different magnetic fields, pointing out of the paper. The curvature is indeed in the same direction as for a negative discharge (see fig. 6.2). Also in this case the curvature reverses direction upon changing the field direction (not shown). These data confirm at least qualitatively the assumption that the discharge path is directly related to the direction of the drift velocity. On the basis of the same assumption it is possible to calculate Θ_H from the data by comparing the observed path with the calculated direction of the drift. We have used the following equations for

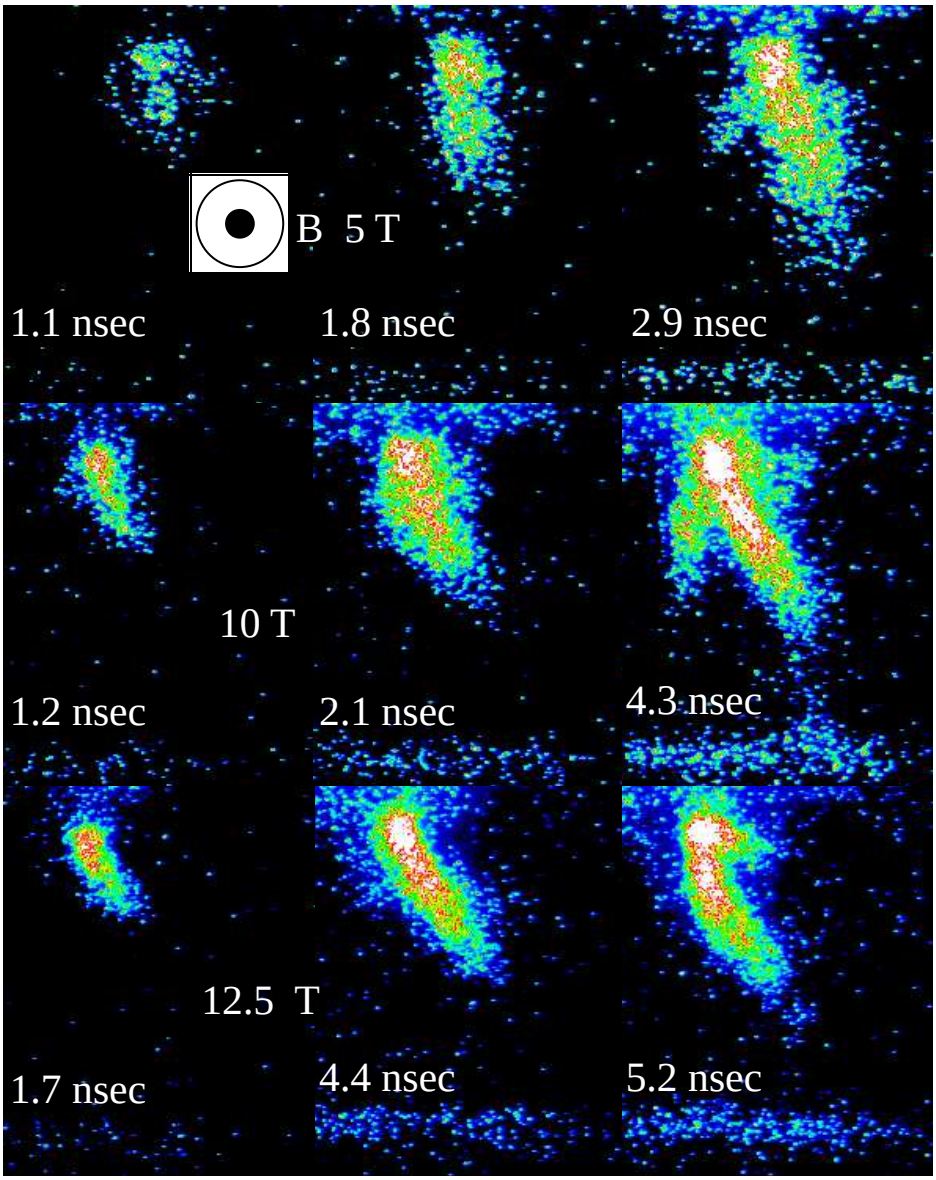

Figure 6.2: Discharge evolution at different magnetic fields, directed towards the reader, at 200 Torr and -40 kV.

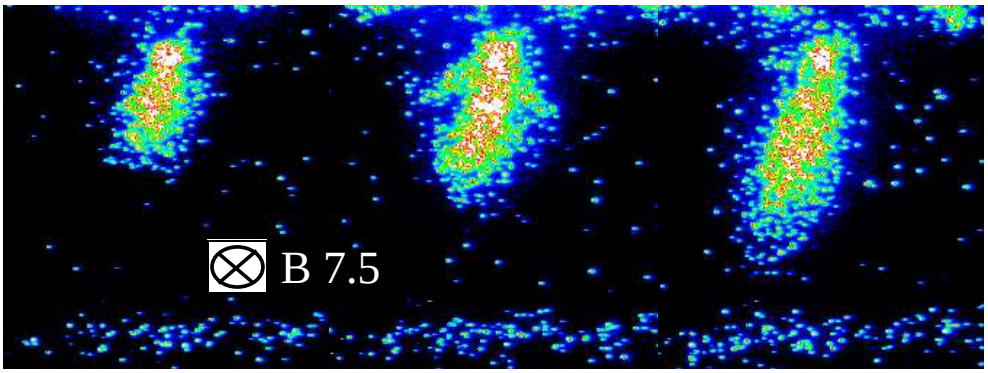

Figure 6.3: Streamer propagation at 7.5 Tesla, directed into the paper, at 400 Torr and -40 kV.

the applied electric field in the point-plate geometry:

$$E_x = \frac{q}{4\pi\epsilon_0} \cdot \left(\frac{x}{(x^2 + (z - a)^2)^{\frac{3}{2}}} - \frac{x}{(x^2 + (z + a)^2)^{\frac{3}{2}}}\right) \tag{6.4}$$

$$E_z = \frac{q}{4\pi\epsilon_0} \cdot \left(\frac{z - a)}{(x^2 + (z - a)^2)^{\frac{3}{2}}} - \frac{z + a)}{(x^2 + (z + a)^2)^{\frac{3}{2}}}\right) \tag{6.5}$$

with a is the distance from the plate to the point electrode. These equations determine the direction of the electric field [2] and the angle (α) of the electric field with the z-direction.

$$\alpha = \arctan\frac{\mathrm{E_x}}{\mathrm{E_z}} \tag{6.6}$$

By adding Θ_H to α the direction of the discharge trajectory is obtained in cartesian coordinates. In fig. 6.5 a few examples of calculated paths are displayed and compared to the path of an experimental discharge pattern, obtained by plotting the trace of the emission peak intensity. Although there is some uncertainty in the measured trajectory, fig 6.5 shows that there is a narrow range of possible values of the Hall angle that describes the data especially at the first stages of the discharge.

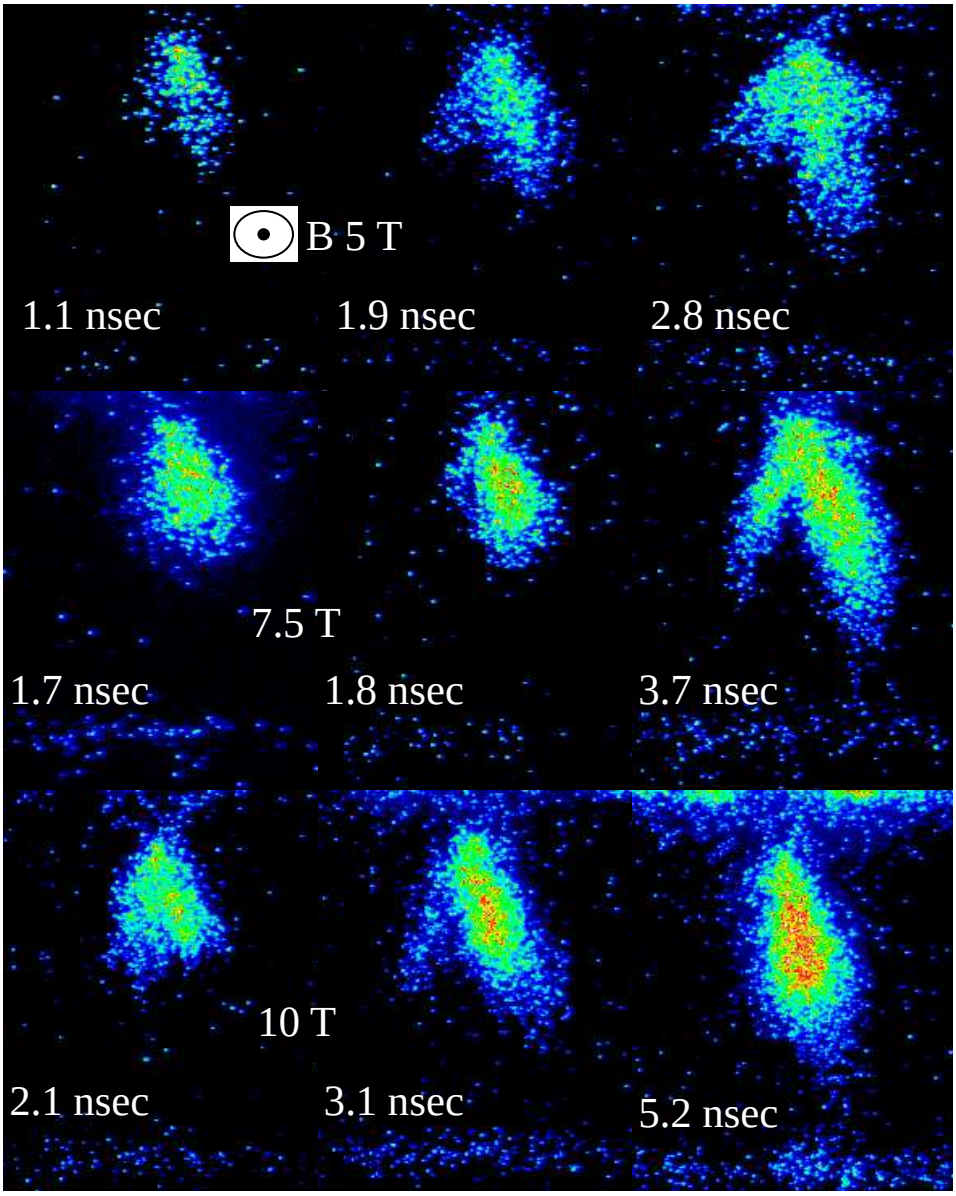

Figure 6.4: Discharge evolution at different magnetic fields at 400 Torr and 40 kV.

After about 7 mm, in this example, the direction of the path is clearly changing. We believe that this observation is a direct manifestation of the fact that first the streamer path is determined by the applied field, while after a certain distance (7 mm in this case) the electric field of the streamer itself is determining the path and the applied field does not play a major role anymore.
We have systematically determined Θ_H from fitting measured traces, such as the one in fig. 6.5 as a function of magnetic field, pressure and applied voltage. The results (fig. 6.6) display an angle Θ_H that increases linearly with increasing magnetic field, as expected from eq.

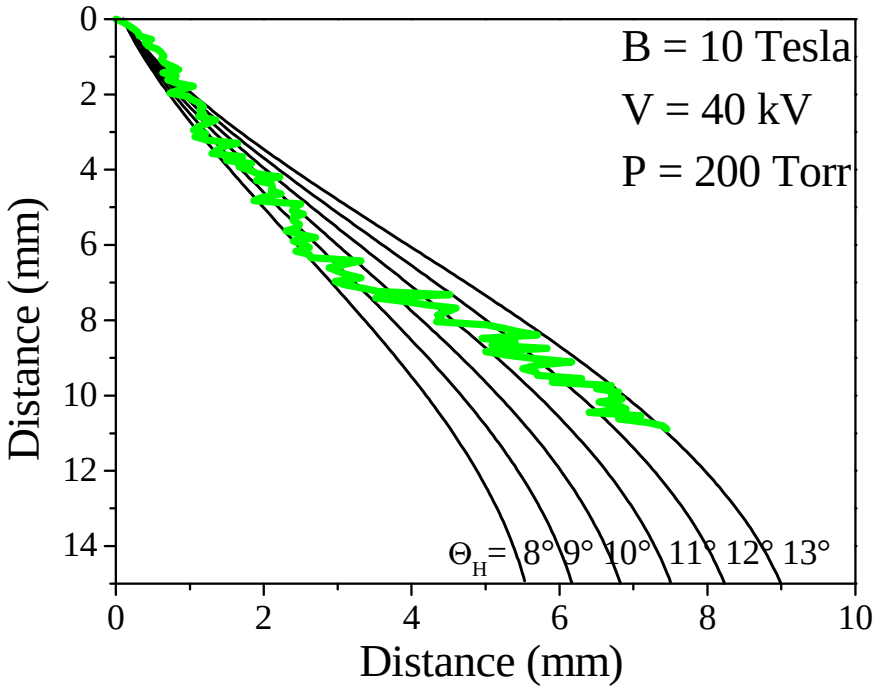

Figure 6.5: The calculated paths for streamer propagation (the black lines) for different values of the Hall angle and the measured path of the streamer (grey line).

6.3. On the other hand Θ_H should also depend on τ (the average time in between collisions) and therefore on the pressure which has not been observed in the experiment (see fig. 6.6). At present we have no satisfying explanation for this behavior.
From eq. 6.3 it follows that the absolute value of E and its direction are not important for the Hall angle. Indeed the insert of fig. 6.6 clearly shows that Θ_H stays constant for all the electric fields. This observation is also consistent with the assumption that the discharge path is determined by the drift velocity.
From the slope of the experimentally obtained magnetic field dependence

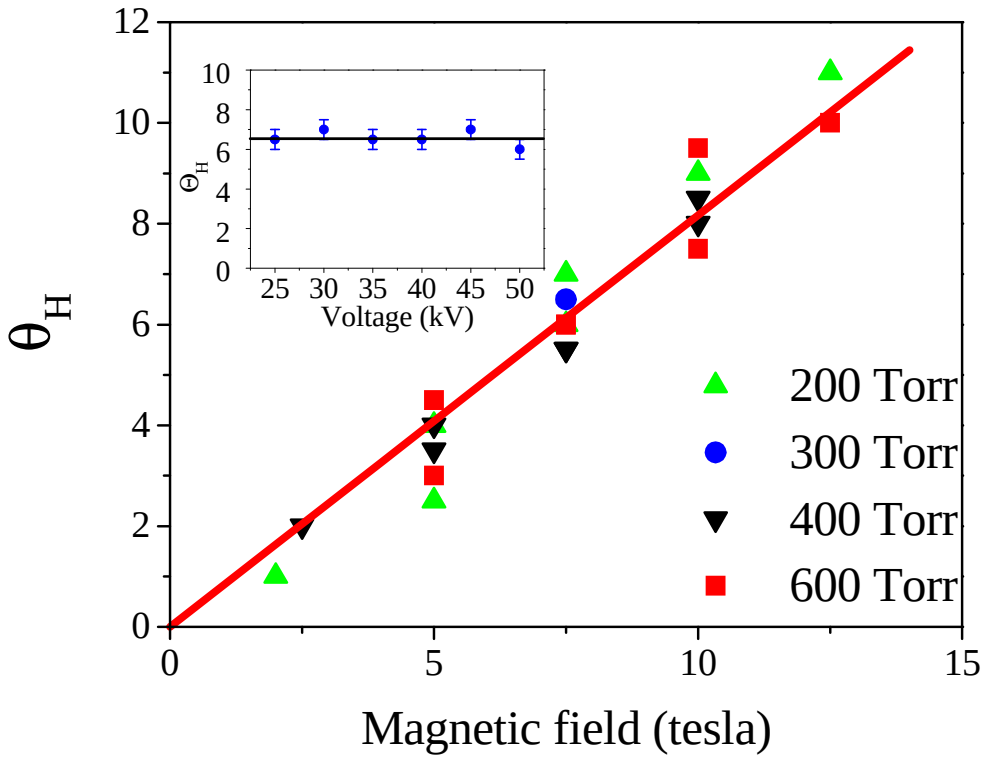

Figure 6.6: The Θ_H as a function of magnetic field for different pressures for positive and negative voltage. In the insert Θ_H as a function of electric field, at 300 Torr and 7.5 Tesla.

(fig. 6.6) of Θ_H, and using eq 6.3 we estimate τ to be $1 \cdot 10^{-13}$. This value is to be compared to the time an electron needs to be accelerated in the given electric field, to obtain sufficiently high kinetic energy for ionization. A simple calculation shows that in an applied electric field of 40kV/15mm it takes $5 \cdot 10^{-12}$s to accelerate an electron to an energy of 15 eV, that is need to ionize N_2 (fig. 3.10). This time is about twenty times longer than the average time between collisions, inferred from the Hall angle. This result is quite reasonable since most collisions will not lead to ionization. From our estimations it appears that only every twentieth collision leads to ionization.

6.2 Conclusion

The measured path of discharges in a perpendicular magnetic field show a curvature which is independent of the direction and the magnitude of the applied electric field. Furthermore the initial phase of the discharge trajectory is well described assuming that the path reflects the electron drift velocity. Calculated paths for different Hall angles Θ_H reasonable well reproduce the discharge pattern and explain the experimental data. The same analysis for different pressures shows that the Hall angle is independent of the pressure. Since the scattering time τ enters in the Hall angle and is expected to depend strongly on pressure, we cannot explain this observation in a simple manner.
At longer distances from the tip the curvature of the discharge could not be fitted anymore with a constant Hall angle. We believe that these data show that after a certain distance the electric field caused by the streamer itself starts playing a major role in the development of the streamer and overrules the applied field. This conclusion is consistent with the conclusion drawn earlier in chapters 4 and 5 on the basis of an analysis of the shape and propagation velocity of the discharge.
Finally we can conclude that photoionization does not seem to play a major role in the evolution of the discharge. Photoionization would determine the path by preionizing atoms in front of the tip, while the propagating front will then proceed towards this preionized regions. Since photon propagation is not influenced by the presence of a magnetic field, this

preionization and thus the discharge path should be field independent.

6.3 Bibliography

[1] O.M. Corbino, Phys. Z. **14** (1911), 561.

[2] I.S. Grant, and W.R. Philips *Electromagnetism* (1990).

Part II

Quantized Conduction

Chapter 7

Quantized conduction in Au nanocontacts

Introduction

The electron transport through metallic nanostructures such as nanowires and nanoparticles continues to attract significant attention. Among recent important observations, it has been demonstrated that just before the electric contact between two pieces of a simple metal is broken, its conductance is quantized at approximately integer multiples of $G_0 = 2e^2/h$. This quantization has been observed by scanning tunnelling microscopy [1,2,3] and using mechanically-controllable break-junctions [4] as well as in more simple, table-top experiments using touching gold wires [5] and relay contacts [6]. In all these experiments, a mechanical nanocontact (a narrow metallic neck) is formed at the final stages of the separation of two macroscopic electrodes. When the electrodes are pulled apart, the metallic neck stretches out until it contains only a few atomic rows [7]. At this, late stage of the separation of the electrodes, the contact conductance exhibits the quantized values corresponding to the number of atom rows left in the nanowire [4,7].
The simplest way to observe the conductance quantization in such atomic wires is to measure the transient conductance during the process of breaking a mechanical contact between two gold electrodes. Such

transient conductance traces exhibit a step-like behavior with plateaus around the quantized values [5,6]. It is important to emphasize that the conductance quantization observed in nanowires is always statistical in nature, which means that the conductance plateaus appear with a finite spread around integer values. This spread is due to random deviations from the ideal transmission for electrons travelling through the wire and originates from incidental differences in the quality of drawn wires. It is shown that backscattering processes in the nanoneck, due to impurities, disorder and boundary corrugations, give rise to differences in plateau's lengths and positions [8-12]. To study quantized properties of the nanowires obtained using the breaking contact, it has become standard to measure histograms, which show the relative occurrence frequency of various conductance values [3-6].
In this chapter, we report the effect of high magnetic fields on this type of conductance quantization using Au contacts at room temperature. We find that in a magnetic field the conductance quantization still exists which is already amazing, and that the quantization becomes significantly better defined in strong fields applied parallel to the probing current. This unexpected improvement is accompanied by a shorter average length of the drawn nanowires. In contrast, a strong perpendicular field is found to make the electric contact unstable, preventing the observation of conductance quantization.

7.1 Experimental setup

In our experimental setup, shown in fig. 7.1, the electric contact is formed between a sharp tip (100 μm wire) and a massive plate, both made from pure polycrystalline Au and set under ambient conditions. The gold plate is fixed and the tip is moved by a piezoelectric actuator driven by voltage pulses of a triangular shape. The tip speed is controlled by the amplitude and frequency of the pulses and kept constant during the experiments. The voltage drop across the Au contact is measured by a Yokogawa DL1540 oscilloscope, with a 150 MHz bandwidth and a 200 Msample/s sampling rate. The data acquisition is triggered when the voltage exceeds a predetermined value. Using computer control, it is possible to obtain 1500

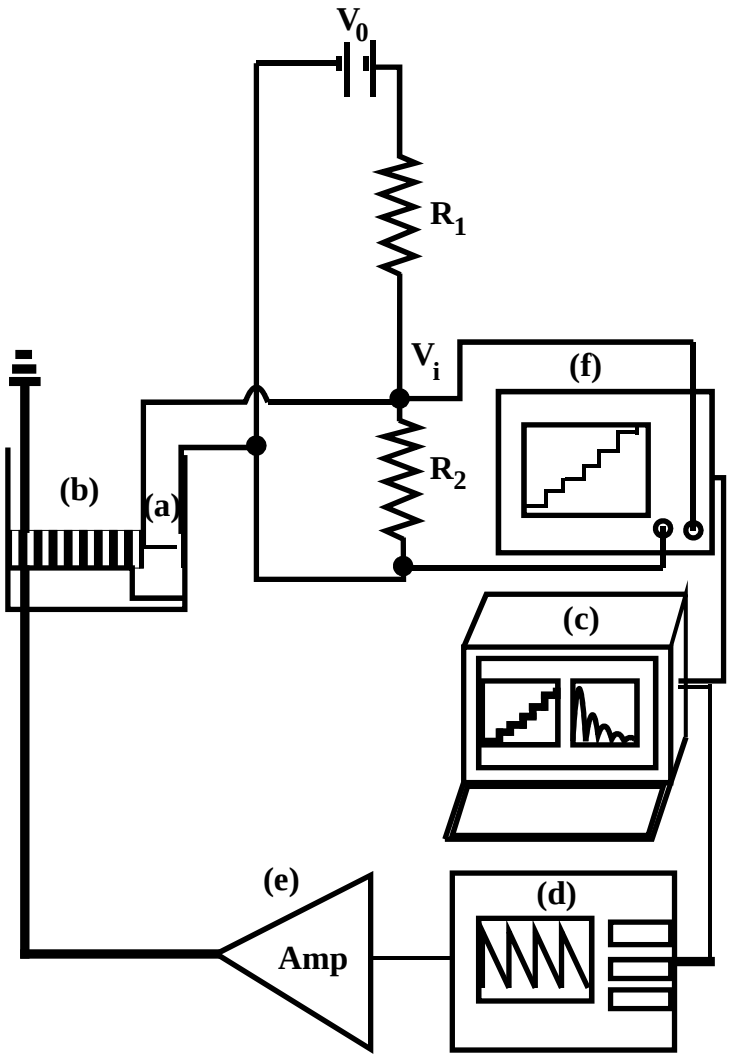

Figure 7.1: The experimental setup. The gold wire and plate (a) move in and out of contact by a piezo (b). The computer (c) controls the measuring cycle, which starts from giving a triangular pulse by the pulse generator (d), to the amplifier (e) and then to the piezo. The voltage is measured over the voltage divider (V_i) on the oscilloscope (f). The voltage V_0 is 15 Volt and $R_1 = 400\Omega$ and $R_2 = 40\Omega$ are used as a voltage divider.

measurements per hour while analyzing and displaying the resulting histogram in real time. Typically, 6000 curves are analyzed to obtain a reliable histogram.
The conductance through the contact is found by measuring the voltage drop across the contact. The current through the contact is limited to 10-60 μA by proper choice of R_1. Typical values of the resistances are R_1=400 kΩ and R_2 = 40 kΩ. In the further analysis of the traces the voltage (V_i) values are transformed into corresponding conductance values G_i using the equation

$$G_i = \frac{I_0}{V_i} \; - \; G_R \tag{7.1}$$

where the current I_0 and the conductance G_R can be found from the circuit in fig. 7.1 as I_0=V_0/R_1 and G_R=$(1/R_1 + 1/R_2)$. To achieve the required high resolution over a wide range of conductances we measure simultaneously on two input lines of the oscilloscope with different sensitivity settings.

7.2 Conduction measurements in magnetic field

With the help of the piezo element the gold tip is pushed against the gold plate. Then it is retracted back and during the breaking of the contact the conduction is measured. In fig 7.2 the conduction is shown. The first thing which can be seen in this figure is that all the lines are different. Furthermore it is clear that there are steps inside the lines. How is this possible?
When the characteristic length scale of a conductor is reduced below the mean free path of the electrons at the Fermi surface, the ballistic transport regime is entered. In this regime, the electrons will predominantly be scattered from the boundaries of the constricting geometry. A quantum point contact (QPC) is a ballistic point contact between two macroscopic bodies where the width is so small that it is comparable to the Fermi wavelength. In a QPC, the quantum-mechanical wave character of the electrons becomes important, thus giving the possibility of observing ex-

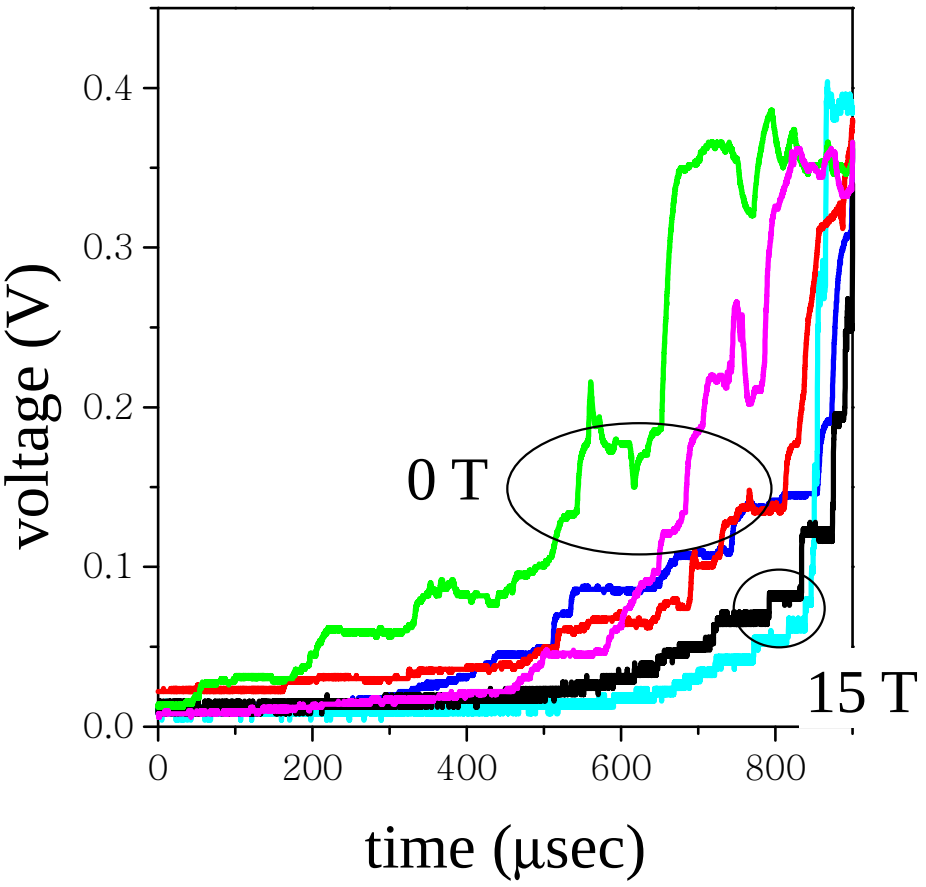

Figure 7.2: Conduction measurements during the retraction of the gold tip for 0 T and 15 T.

citing quantum phenomena like quantized conductance.
In a QPC, the conductance G can be calculated using the Landauer formula [13]. B*ü*ttiker, simplified the Landauer formula by the use of so-called eigenchannels, which do not mix in the scattering region of the QPC [14], the Landauer formula then is:

$$G = G_0 \sum_i T_i \tag{7.2}$$

where T_i denotes the transmission probability of the ith eigenchannel and $G_0 = 2e^2/h \approx 1/(12.9k\Omega)$ is the fundamental quantum unit of conductance.

If the cross section of the QPC varies slowly along the constriction, the transmission probability of single channels T_i will be either 1 or 0 [6, 10]. Here we neglect the smearing due to finite temperatures as well as any effects caused by internal disorder and inelastic impurity scattering. When these criteria are fulfilled, the sum of transmission probabilities will attain integer values, and thus the conductance will be quantized in units of G_0. This is the reason that there are steps in the conductance measurements of fig. 7.2. The measurements are done at room temperature, so there will be disorder and scattering of impurities that is why every line in this figure is different. But it is still possible to get the integer values out of the measurements by making histograms.

Fig. 7.3 plots the conductance histograms obtained in zero magnetic field, 5 T and 15 T applied parallel to the probing current. Three peaks at 0.98 G_0, 1.9 G_0 and 2.8 G_0 are clearly seen in the histogram. The position of the conductance peaks is not exactly at integer values because electron states in Au are slightly bound, i.e. they are not free electron states, which is required for the exact quantization in units G_0 [15]. The observed peak positions are in good agreement with earlier reports for Au [4,5,6]. As clearly seen in fig. 7.3, the quantization still existed in strong magnetic fields and the peaks stay at the same position but the shape is changing, the peaks get narrower and the valleys deeper as a function of magnetic field, indicating that conductance plateaus at random values occur less frequently.

If the magnetic field is applied perpendicular to the probing current, there is little effect on histograms up to 5 Tesla but in higher fields the contact between the tip and the plate becomes unstable, as witnessed by huge voltage fluctuations.

In fig. 7.4 we show the influence of the value of the probing current on the quality of conductance histograms in parallel magnetic field. It can be seen that in high fields, the quantization is considerably improved as we increased the probing current from 13μA to 52 μA. On the other hand, in zero field we find no difference between the low and high currents. Note that we have used sufficiently low currents in order not to enter in a qualitatively different (non-linear) regime [16].

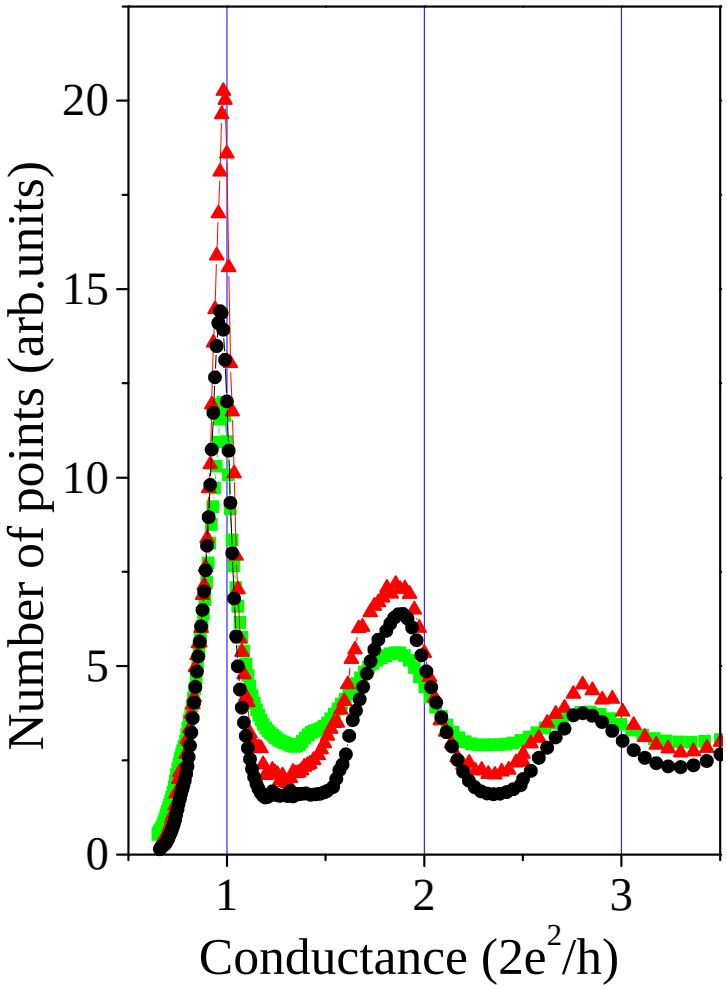

Figure 7.3: Conductance histogram for 6000 breaks of the electric contact in 0 T (squares), 5 T (triangulares) and 15 T (circles). The magnetic field is parallel to the probing current.

To get more qualitative information we analyzed the extent to which the nanowires, that contribute to the conductance histograms, stretch with and without magnetic field. In our experiments, we cannot measure the length of the nanowires but it is reasonable to assume that the longer the drawn wire the longer distance the piezo has to travel before the wire is

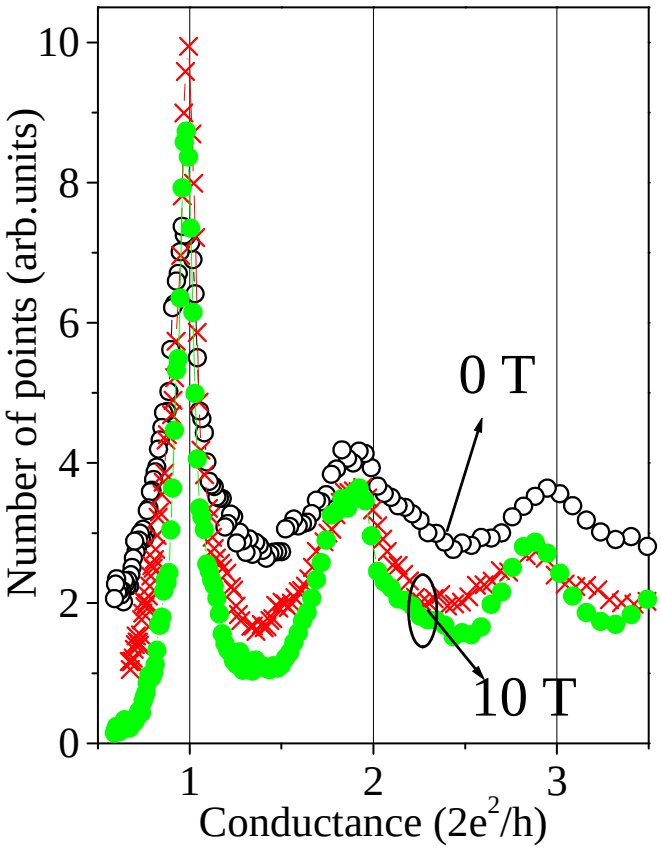

Figure 7.4: Conductance histograms for different probing currents and magnetic fields. The open and closed circles are for 52 μA in 0 and 10 T, respectively; the crosses for 13 μA in 10 T.

torn apart. In fact, long wires can have many places (necks) at which they plastically creep under tearing force of the piezo driver. On the other hand, short straight wires with a single neck can be stretched at a minimum distance. Fig 7.2 shows that indeed typical transient curves become significantly steeper with increasing magnetic field. As the magnetic field does not influence the operation of the piezo driver, the only possible conclusion is that the nanowires that are sampled on our conductance histograms, stretch significantly less in strong fields. For a quantitative

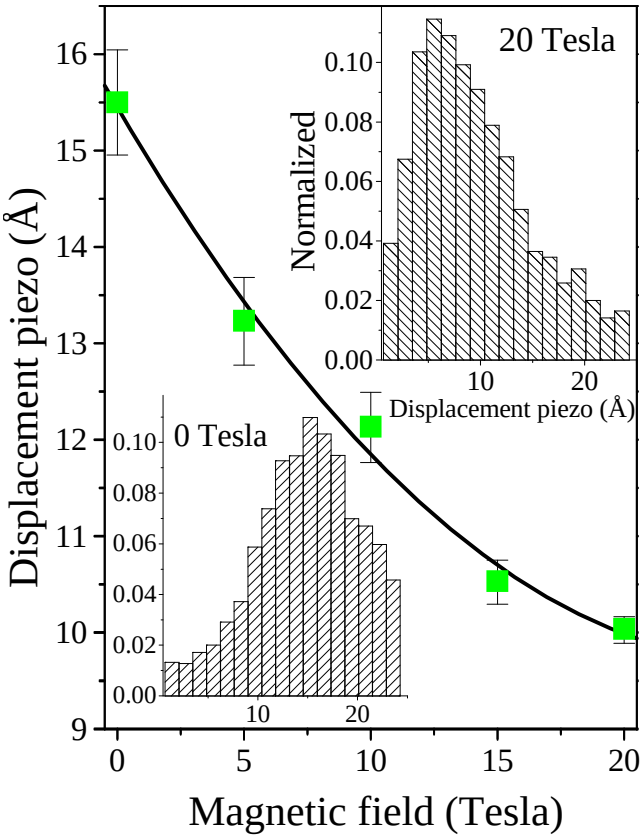

Figure 7.5: The average displacement of the piezo required for breaking the contact as a function of magnetic field. The insets show the distribution of this displacement for 0 T and 20 T.

analysis, fig. 7.5 plots the average displacement of the piezo required to break a nanowire. Here we have chosen, for simplicity 6 G_0 as the starting point for the measured displacement process (at this value the first peak like feature becomes noticeable on our histograms). In fig. 7.5, the average length of the sampled nanowires becomes increasingly shorter with increasing parallel magnetic field. One can see that at B=0 the histogram of the wires length exhibits a maximum at 15 Å while at B=20T the maximum shifts to 6 Å. This allows use to conclude that with increasing magnetic field, we measure histograms of increasingly shorter wires.

Summarizing the experimental results we find that the conductance amazingly still existed in high magnetic fields and that the quantization is becoming increasingly better by higher parallel magnetic field and with higher currents.

7.3 Conclusions

The improvement of the conductance is accompanied by a shorter length of the wires. So there are 3 parameters, *B, I* and *l*.
All three parameters are present in the Lorentz force:

$$F_L = I\ l\ B\ \sin\alpha \tag{7.3}$$

where I is the probing current through the wire, l is the wire's length, B is the magnetic field and α is the angle between the magnetic field and current. If the magnetic field is applied perpendicular to the current ($\alpha = 90°$) and the force acts on the entire length of the Au tip (100 μm in our case), Eq 7.3 yields the force of 100 nN for a typical current of 50 μA at 20 Tesla.
If the magnetic field is parallel to the current (α=0), the tip experiences no Lorentz force. However, we cannot exclude a slight misalignment of the tip and the field (2 to 3°). In addition, the drawn nanowires can be expected to be inclined with respect to the tip and field directions. The longer the wire, the more likely the wire or a part of it goes under a small angle. Assuming $\alpha = 3°$ and taking several inter-atomic distances (10 Å) for the minimal possible length of a misaligned segment of a nanowire, the Lorentz force acting on the corresponding atoms appears to be 5×10^{-14}N.
In the perpendicular case the whole tip is moved, so we need to calculated the displacement of the tip. To calculated this displacement we use the following formula

$$y = \frac{w \cdot l^3}{3 \cdot E \cdot \frac{\Pi \cdot d^4}{64}} \tag{7.4}$$

In which l is the length, d the diameter, E the elasticity ($79 \cdot 10^9 N/m^2$) and W the force. For the perpendicular case the displacement is 10^{-13}m, which is very small.
For the parallel case it is found [17] that the force needed to break a gold

chain is 2×10^{-9}N. So in both case the force is order of 4 to small to break or move the wires.
So the Lorentz force is too small to move or break the nanowires. Because we cannot really see how the breaking of the wires happens we have to speculate what is going on. Of course we tested our setup completely. So we can rule out effects like, current loops, changing of leads and movement of the wires because of movement of the magnet.
The magnetic field does not have so much effect on atoms, but it has a big effect on electrons. Because of the magnetic field tunnelling is much more difficult and it is also possible that the electrons are more focused so they move more through straight wires and almost not through wires which are inclined with respect to the tip.
Another thing is that there are more forces than just Lorentz force acting on the wires. Their is also current-induced force [18] acting on the wires. This force arise because of electron scattering at defects and is also linear with current. It creates a weak bond in the chain and lowers the ultimate tensile strength of the chain, this dramatically increase the probability of thermally activated fracture. In the normal case this force is so small, in the time scale we measure, that there is no effect. But small changes in the geometry result in dramatic changes in stability.
So when the conductance is not perfect, the current-induced force is getting bigger, because there is more scattering and there is a Lorentz force acting on the atoms/electrons. This Lorentz force is the biggest at the atoms near the end, so this will increase the current-induced force. So both forces are helping each other, and this can lead to the observed experimental results, but this is speculation.
In summary, we have studied the conductance quantization in gold point contacts under the influence of strong magnetic fields. The magnetic field perpendicular to the probing current causes little effect in small fields but in higher fields the quantization is completely destroyed because nanocontacts becomes unstable. On the other hand, a magnetic field parallel to the probing current significantly improves the quality of the observed quantization. This unexpected improvement depends also on the current and is accompanied by a shorter average length of the drawn nanowires. We attribute this surprising result to a selection by magnetic field of point contacts with better quantization. This happens, at the final stages of the breaking process.

7.4 Bibliography

[1] N. Agraït, J.G. Rodrigo, and S. Vieira, Phys. Rev. B **47**, 12345 (1993).

[2] J.I. Pascual, J. Méndez, J. Gómez-Herrero, A.M. Baró, N. García, and Vu Thien Binh, Phys. Rev. Lett. **71**, 1852 (1993).

[3] L. Olesen, E. Laegsgaard, I. Stensgaard, F. Besenbacher, J. Schiϕtz, P. Stolze, K.W. Jacobsen, and J.K. Nϕrskov, Phys. Rev. Lett. **72** 2251 (1994).

[4] J.M. Krans, J.M. van Ruitenbeek, V.V. Fisun, I.K. Yanson, and L.J. de Jongh, Nature (London) **375**, 767 (1995); J.M. Krans, C.J. Muller, I.K. Yanson, Th. C.M. Govaert, R. Hesper, and J.M. van Ruitenbeek, Phys. Rev B **48**, 14721 (1993).

[5] J.L. Costa-Krämer, N. García, P. García-Mochales, and P.A. Serena, Surf. Sci. **342**, L1144 (1995).

[6] K. Hansen, E Laegsgaard, I. Stensgaard, and F. Besenbacher, Phys. Rev. B **56**, 2208 (1997).

[7] Hideaki Ohnishi, Yukihito Kondo, and Kunio Takayanagi, Nature (London) **395**, 780 (1998).

[8] A.M. Bratkovsky, A.P. Sutton, and T.N. Todorov, Phys. Rev. B **52**, 5036 (1995).

[9] A.M. Bratkovsky, and S.N. Rashkeev, Phys. Rev. B **53**, 13074 (1996).

[10] M. Brandbye, K.W. Jacobsen, and J.K. Nϕrskov, Phys. Rev. B **55**, 2637 (1997).

[11] P. García-Mochales, and P.A. Serena, Phys. Rev. Lett. **79**, 2316 (1997).

[12] W.B.Jian, C.S. Chang, W.Y. Li, and T.T. Tsong, Phys. Rev. B **59**, 3168 (1999).

[13] R. Landauer, IBM J. res. Dev. **1**, 223 (1957); J. Phys. C **1**, 8099 (1989); M. Büttiker, Y. Imry, R. Landauer, and S. Pinhas, Phys. Rev. B **31**, 6207 (1985).

[14] M. Büttiker, IBM J. res. Dev. **23**, 63 (1988).

[15] P. García-Mochales, P.A. Serena, N. García, and J.L. Costa-Krämer, Phys. Rev. B **53**, 10268 (1996).

[16] K. Itakura, K. Yuki, S. Kurokawa, H. Yasuda, and A. Sakai, Phys. Rev. B **60**, 11163 (1999).

[17] G.Rubio, N.Agraït, and S. Vieira, Phys. Rev. Lett. **76**, 2302 (1996).

[18] T.N. Todorov, J. Hoekstra, and A.P. Sutton, Phys. Rev. Lett. **86**, 3606 (2001).

Summary

In this thesis the transition from an electrical conductor to isolator, and vice versa, is studied. This transition is a typical example of a strongly non-linear process. Two different types of systems are used in order to realize and study both the transition from isolator to conductor, as well as from conductor to isolator. Part I of the thesis deals with experiments in which a gas (nitrogen), which is a good isolator under normal conditions, is transformed in a good conductor by application of a high electric field. In part II the opposite process is discussed, by measuring the conductance of a small gold contact during the moment it breaks, and the conductance disappears.
The thesis starts with a general introduction (chapter 1), including a historical review of some important aspects of conduction. In part I (chapters 2 till 6) gas discharges are investigated, starting off with the discussion of the basic properties of gas discharges and a summary of the open questions and issues that are addressed in this thesis. The most famous type of discharge is obviously lightning, where the air in the earth's atmosphere is ionized and starts to be conductive. The ionized channel heats up and emits light which leads to the beautiful well known pictures. In the laboratory lightnings or discharges are generated by application of a high voltage in between two electrodes, a distance d apart, mounted in a cell filled with gas at pressure p. At low pressures and/or distances ($p * d < 100$ torr*cm) a breakdown can be described by an expression first derived by Townsend, in which the *applied* electric field determines the discharge. For higher values of $p * d$ this description does not apply anymore because also the electric field of the ionized channel becomes important. In this case the breakdown is described in terms of *streamers*, at early times after the first ionization, and *leaders*, when the ionized channel heats up further and constitutes a plasma. In this

thesis particular emphasis is devoted to the propagation of streamers. In some theoretical investigations streamers are described as a typical example of non-linear pattern formation, where the streamer resembles a fingerlike shape, propagating with constant width and shape, and where the ionization is restricted to a small sheet of only a few μm size. However, the precise ionization process, i.e. the role of photo-ionization, and the actual size and shape of the streamer are very controversial issues nowadays, mainly due to the lack of systematic, reliable experimental information. Performing such type of experiments is a difficult task because the formation and propagation of streamers occurs on very short (nanosecond) timescale. Moreover, due to their inherent non-linear character subsequent discharges always differ from each other. The main goal of this thesis is to measure the formation and propagation of streamers, as a function of several experimental parameters, such as electric and magnetic field strengths and gas pressure, by using a newly developed imaging technique utilizing an ultrafast intensified CCD camera.

A detailed description of the experimental technique is presented in chapter 3. An ultrafast intensified CCD camera (shutter time 5 nanoseconds) is used to record time-resolved images of the discharges. Simultaneously the electrical transients are measured, which enables us to monitor the propagation of the discharge with a time-resolution of 0.1 nanosecond. The discharge is generated in between a point-like and a plate-like electrode (15 mm apart), where a high positive or negative voltage is applied to the point-electrode with the plate electrode grounded.

In chapter 4 the images are analyzed. The first images, record shortly after the start of the discharge, reveal that the emission pattern exhibits many, small, point-like, intense spikes, which implies that the ionization process starts at many places at once, in contrast to the finger-like streamers found in computer-simulations. The amount of ionized regions increases significantly with time, which resembles the formation of an ionized channel, but actually this channel consists of localized regions with ions surrounded by free electrons that transfer the potential of the electrode to the front of the discharge. As a consequence, the local electric field distribution of the streamer becomes dominant, which is illustrated by the fact that the images show a considerable amount of branching, especially at high pressures and/or low electric fields. We demonstrate

that branching is less frequent for positive streamers than for negative streamers, which is related to their different mechanism of propagation.
In chapter 5 the propagation velocity of the streamers is studied. The most remarkable observation is that for both polarities the propagation speed is more or less constant, in spite of the fact that the applied electric field strongly varies with the distance to the electrode, due to the point-plate geometry. Indeed if the electrical potential is effectively transferred to the tip of the streamer, the constant propagation velocity of the streamer is determined by the local electric field near the streamer tip, rather than the applied field.
Chapter 6 is devoted to the propagation of streamers under the application of a strong, perpendicular magnetic field. The magnetic field leads to an additional (Lorentz)force on the electrons. By studying the effect of this force on the streamer propagation we collect valuable information regarding the questions whether photo-ionization plays a major role in the streamer propagation, and at which point the local field at the streamer tip becomes more important than the applied field. The measured images reveal that the discharge channels are curved in a magnetic field, and that the curvature increases with field strength. This observation unambiguously proves that photoionization does not play a major role in the evolution of the discharge, since photon propagation is not influenced by a magnetic field. Furthermore, it is found that up to 7 mm from the point-electrode the curvature of the discharge can be described using a constant Hall angle, determined by the applied electric and magnetic fields. At larger distances this is not possible anymore, which shows that at those distances the local field of the streamer tip dominates the applied field.

In part II of the thesis (chapter 7) we study the disappearance of conductivity when a metal contact is interrupted. We demonstrate that just before the electric contact between two gold contact is broken, the conductance disappears in quantized steps of approximately integer multiples of $G_0 = 2e^2/h$. This quantization improves when a magnetic field is applied parallel to the probing current. This improvement depends on the current and is accompanied by a shorter average length of the drawn nanowires. This result can be explained by a selection of point contacts with better quantization, through the magnetic field.

Samenvatting

In dit proefschrift wordt de overgang van een elektrische geleider naar een isolator, en andersom, bestudeerd. Deze overgang is een typisch voorbeeld van een sterk niet-lineair verschijnsel. Er worden twee soorten systemen gebruikt teneinde zowel de overgang van isolator naar geleider als ook van geleider naar isolator te bewerkstelligen en te bestuderen. Deel I van het proefschrift beschrijft experimenten waarbij een gas (stikstof), wat onder normale omstandigheden een goede isolator is, verandert in een goede geleider door een hoog elektrisch veld aan te leggen. In deel II wordt het tegengesteld proces gerealiseerd, door de geleiding door een minuscuul goudcontact te meten op het moment dat het goudcontact breekt en de elektrische geleiding verdwijnt.
Het proefschrift begint met een algemene inleiding (hoofdstuk 1), waarin een kort historisch overzicht gegeven wordt van het voortschrijdend begrip van de fysica van geleiding. Vervolgens worden in hoofdstukken 2 tot en met 6 experimenten beschreven aan gasontladingen. In hoofdstuk 2 worden de basisbegrippen van de gasontladingfysica geïntroduceerd, en worden de openstaande vragen geformuleerd, waarop dit werk een antwoord tracht te vinden. Bliksem is het meest bekende voorbeeld van een gasontlading, waarbij de lucht in de aardatmosfeer geïoniseerd wordt en geleidend wordt. Het geïoniseerde kanaal warmt op en zendt licht uit, wat leidt tot de bekende prachtige lichtverschijnselen. In het laboratorium wordt een bliksem, vonk of gasontlading gemaakt door een hoge spanning aan te leggen tussen twee elektrodes, een afstand d uit elkaar, waartussen zich het gas, met druk p, bevindt. Bij lage druk en/of korte afstand ($p * d < 100$ torr*cm) kan de ontlading beschreven worden door de uitdrukking van Townsend, waarbij voornamelijk het *aangelegde* elektrische veld bepalend is voor de elektrische doorslag. Voor hogere $p * d$-waarden voldoet deze beschrijving niet meer omdat dan ook het elektrische veld

van het geïoniseerde kanaal zelf bepalend wordt voor de vonk. In dit geval spreekt men van zogenaamde *streamers*, in het prille begin van het ionisatieproces, en *leaders*, als het geïoniseerde kanaal verder opwarmt en beschreven kan worden door een plasma. Dit proefschrift bestudeert met name de voortplanting van streamers. In sommige theoretische studies worden streamers opgevat als een typisch voorbeeld van niet-lineaire patroonvorming, waarbij de streamer beschreven wordt als een vingervormig kanaal dat zich met constante breedte en vorm voortbeweegt en waarbij de ionisatie beperkt blijft tot een klein gebied van slechts een paar μm grootte. Het exacte ionisatie proces, zoals de rol van foto-ionisatie, en de precieze vorm en voortplantingssnelheid van de streamer zijn momenteel controversiële onderwerpen, met name vanwege het ontbreken van systematische, experimentele gegevens. Het uitvoeren van zulke experimenten wordt erg bemoeilijkt omdat de vorming en voorplanting van streamers op extreem korte (nanoseconde) tijdschalen gebeurt. Daarnaast zorgt hun sterk niet-lineaire karakter ervoor dat elke opeenvolgende gasontlading anders is. Het hoofddoel van dit proefschrift is om de formatie en voortplanting van streamers experimenteel vast te leggen als functie van diverse experimentele parameters, wat pas met de recente ontwikkeling van ultrasnelle CCD camera's mogelijk is geworden.
De experimentele opstelling wordt uitgebreid beschreven in hoofdstuk 3. Met behulp van een snelle CCD camera (sluitertijd 5 nanoseconde) worden er tijdsopgeloste afbeeldingen gemaakt van gasontladingen in stikstof. Tegelijkertijd worden ook de elektrische signalen nauwkeurig gemeten, wat het mogelijk maakt om uiteindelijk de voortplanting van de streamer te volgen met een tijdsresolutie van 0.1 nanoseconde. De ontlading wordt gecreëerd tussen een puntvormige en een plaatvormige elektrode (op 15 mm afstand), waarbij er een hoge positieve of negatieve spanning op de puntelektrode wordt gezet, met de plaatelektrode aan aarde.
In hoofdstuk 4 worden de afbeeldingen geanalyseerd. De allereerste afbeeldingen, kort na het begin van de gasontlading, laten zien dat het emissiepatroon bestaat uit vele discrete, kleine, intense pieken, waaruit blijkt dat het ionisatieproces op talrijke plaatsen tegelijk start, in tegenstelling tot de vingervormige kanalen uit computersimulaties. Met het verloop van de tijd neemt het aantal geïoniseerde gebieden sterk toe, wat lijkt op de formatie van een geleidend streamerkanaal, maar wat feitelijk bestaat uit vele gelokaliseerde gebieden met ionen met daartussen vrij-

gemaakte elektronen die de elektrische potentiaal overbrengen naar de voorkant van de streamer. De feitelijke locale potentiaalverdeling wordt op dit moment erg belangrijk en zorgt er bijvoorbeeld voor dat er vertakkingen ontstaan aan de voorkant van de ontlading. We laten zien dat dit zowel gebeurt bij positieve als bij negatieve streamers, voornamelijk bij hoge druk en/of laag elektrisch veld. Wel is het zo dat vertakkingen minder vaak voorkomen bij positieve dan bij negatieve streamers, wat verklaard kan worden door de verschillen in het voortplantingsmechanisme.
In hoofdstuk 5 presenteren we metingen van de voortplantingssnelheid van zowel positieve als negatieve streamers. De meest opmerkelijke observatie is dat voor beide polariteiten de snelheid constant is tijdens de voortplanting, dit ondanks het feit dat het aangelegde elektrische veld, vanwege de punt-plaat geometrie, sterk afhangt van de afstand tot de puntelektrode. Deze observatie kan verklaard worden door het feit dat het elektrische veld van de elektrode inderdaad effectief wordt overgebracht naar de voorkant van de elektrode en dat dit locale elektrisch veld, en niet langer het aangelegde elektrisch veld, de voortplantingssnelheid bepaalt.
Hoofdstuk 6 handelt tenslotte over gasontladingen in een sterk, loodrecht aangelegd, magneetveld. Het magneetveld zorgt voor een extra (Lorentz)kracht op de bewegende elektronen in de ontlading. Door de uitwerking van deze kracht op de ontlading vast te leggen verkrijgen we belangrijke informatie betreffende de vragen of foto-ionisatie een belangrijke rol speelt bij de voortplanting van de streamer en op welk punt het aangelegde elektrische veld ondergeschikt wordt aan het elektrische veld van de ruimtelading van de streamer. De gemeten afbeeldingen laten zien dat het ontladingskanaal gebogen wordt door het magneetveld, wat bewijst dat foto-ionisatie geen belangrijke rol kan spelen, aangezien de voortplanting van licht niet beïnvloed wordt door een magneetveld. Tevens is gebleken dat tot op 7 mm van de puntelektrode de buiging van de ontlading omschreven kan worden door een constante Hall hoek tussen de aangelegde elektrische en magnetische velden. Hierna is dit niet meer mogelijk, wat aantoont dat na deze afstand het elektrische veld van de streamer zelf de voorplanting van de streamer gaat bepalen.
In deel II van het proefschrift (hoofdstuk 7) bestuderen we het verdwijnen van de geleiding wanneer een metaalcontact wordt verbroken. We laten zien dat net voordat het elektrische contact tussen twee goud contacten wordt verbroken de geleiding gekwantiseerd is in ongeveer gehele

veelvouden van $G_0 = 2e^2/h$. Deze kwantisatie verbetert als een magneetveld parallel aan de stroom geplaatst wordt. Deze verbetering hangt af van de stroom en wordt vergezeld met een gemiddeld kortere lengte van de getrokken nanodraden. Dit resultaat kan verklaard worden door een selectie van puntcontacten met een betere kwantisatie door het magneetveld.

Publications

- *Breaking of time-reversal symmetry probed by optical Second-harmonic Generation*
  R. Stolle, K.J. Veentra, F. Manders, N. Persat, H. van den Berg and Th. Rasing
  Phys. Rev. B **55**, R4925 (1997).

- *Second Harmonic Generation study of Quantum Well States and interdiffusion in a Co/Rh multilayer*
  F. Manders, K.J. Veenstra, A. Kirilyuk, H. van den Berg and Th. Rasing
  IEEE transaction on magnets **34**, 855 (1998).

- *Interdiffusion and magnetism of the Co/Rh interface studied by magnetization induced Second Harmonic Generation*
  F. Manders, K.J. Veenstra, A. Kirilyuk, H. van den Berg and Th. Rasing
  Appl. Phys. Lett **73**, 3601 (1998).

- *Improved conductance quantization in gold point contacts in high magnetic fields*
  F. Manders, A.K. Geim and J.C. Maan
  Physica B **294**, 332 (2001).

- *Nonlinear optical and electrostatic force microscopy for ferroelectric polarization imaging*
  E.D. Mishina, N.E. Sherstyuk, K.A. Vorostilov, A.S. Sigov, R. Barberi, M.P. Moret, F. Manders, M.P. de Santo, P.K. Larsen and Th. Rasing
  Appl. Phys B **74**, 783 (2002).

Curriculum Vitae

Freddy Manders werd geboren op 19 juli 1974 te Sittard. In 1992 behaalde hij het VWO diploma aan het Bisschoppelijk College te Echt. Van 1992 tot 1997 studeerde hij natuurkunde aan de Universiteit van Nijmegen. Zijn afstudeerrichting was toegepaste fysica en zijn afstudeerwerk deed hij bij de vakgroep Vaste Stof Fysica II onder leiding van Prof dr. Th. Rasing. Hij studeerde af op het onderwerp tweede harmonische generatie aan het Co/Rh grensvlak. Van 1997 tot 2002 was hij in dienst van de Nederlandse organisatie voor Wetenschappelijk Onderzoek (NWO), als onderzoeker in opleiding (OIO) verbonden aan de Katholieke Universiteit Nijmegen. Daar deed hij onder leiding van Prof. Dr. Ir. J.C. Maan promotieonderzoek naar het ontstaan en voortbewegen van gasontladingen. De belangrijkste resultaten van dat onderzoek staan in dit proefschrift beschreven.